Yuan *et al. Biochar (2026) 8:30*
https://doi.org/10.1007/s42773-025-00540-5

Biochar

ORIGINAL RESEARCH

Open Access

Phosphorus-modified biochar from salvia miltiorrhiza dregs: synthesis, characterization, and dual-functional synergy for heavy metal immobilization and soil fertility augmentation

Jiandan Yuan[1,2], Yanling Liu[1], Qian He[1], Hongting Wen[1], Zhenghua Li[1], Ruifeng Lin[1], Tianzhe Chu[1], Cheng Peng[1*], Chuan Zheng[3,4*], Hulan Chen[1,5*] and Yuzhu Tan[1*]

Abstract

Phosphorus-modified biochar (3K-BC) was prepared from Salvia miltiorrhiza dregs via phosphate modification and applied for lead (Pb) and cadmium (Cd) removal from aqueous solutions and soil. The successful incorporation of orthophosphate into the biochar was confirmed by ^{31}P NMR and other analytical techniques. Solution-based experiments showed that 3K-BC followed pseudo-second-order kinetics and best fitted the Langmuir isotherm model, indicating multiple chemical adsorption processes. The maximum adsorption capacities for Pb and Cd were 361.82 and 123.03 mg g^{-1}, respectively. The adsorption mechanism involved physical adsorption, precipitation, complexation with oxygen-containing functional groups, and cation exchange. Soil experiments demonstrated that 3K-BC significantly reduced heavy metal (HM) bioavailability, with greater reductions at higher application rates. Speciation analysis revealed a decrease in the acid-soluble fraction of Pb and Cd, while their stable, residual forms increased, effectively reducing metal mobility. Further confirmation was obtained through pot experiments, which showed that the application of 3K-BC increased the yield of *Ligusticum chuanxiong* by 61% and promoted its growth. In addition, the concentration of ligustilide increased from 24.24 to 29.63 mg g^{-1}. Under the condition of HM pollution, the total effective components of *Ligusticum chuanxiong* in the experimental group increased by 22.1%. This study provides a simple and effective strategy for remediating Pb- and Cd-contaminated water and soil while simultaneously recycling agricultural waste, thereby serving a dual purpose.

Highlights

- Phosphorus-modified biochar (3K-BC) adsorbs 361.82 mg g^{-1} Pb and 123.03 mg g^{-1} Cd.
- 3K-BC cuts Pb/Cd bioavailability by 93%, stabilizing metals and reducing ecological risk.
- 3K-BC boosts *Ligusticum chuanxiong* yield by 61% while limiting heavy metal uptake.
- Converting herbal residues into biochar supports pollution control and soil fertility.

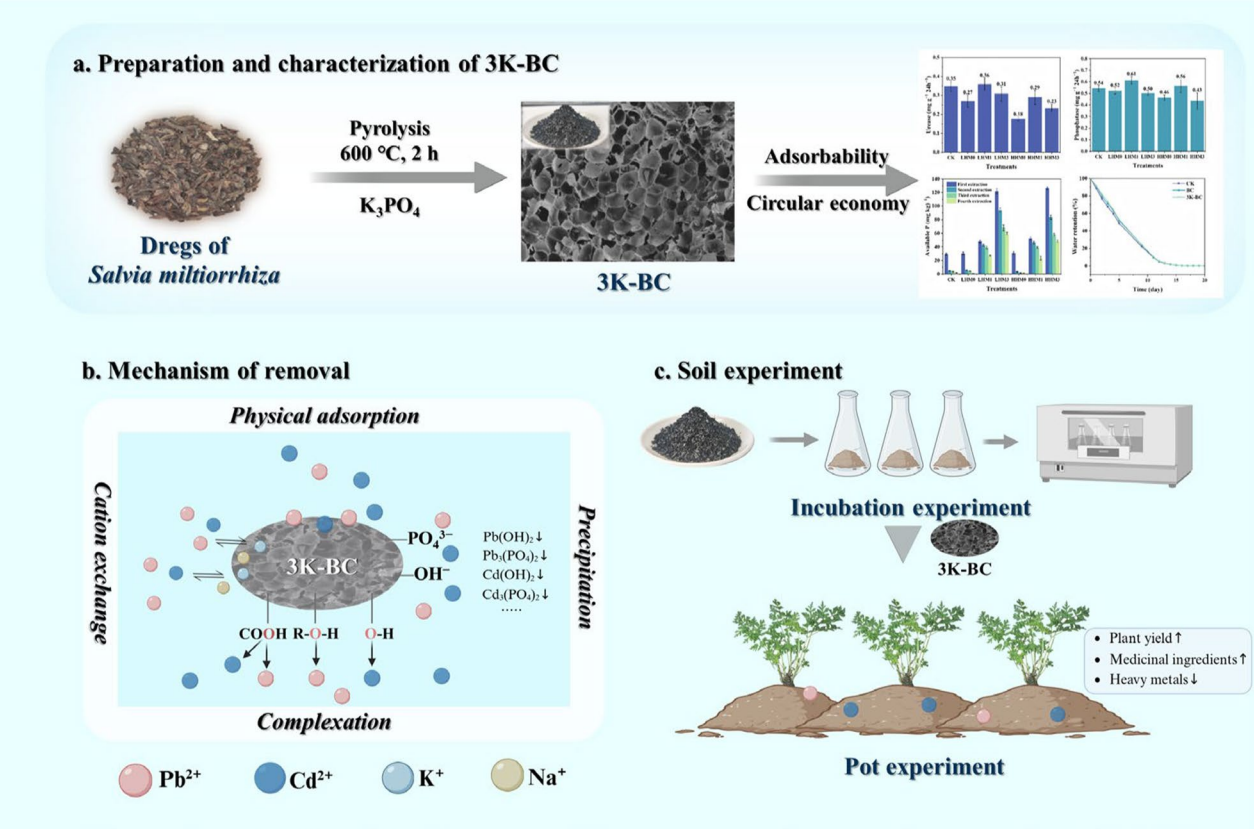
*Correspondence:
Cheng Peng
pc@cdutcm.edu.cn
Chuan Zheng
zhengchuan@cdutcm.edu.cn
Hulan Chen
chenhulan@cdutcm.edu.cn
Yuzhu Tan
tanyuzhu@cdutcm.edu.cn
Full list of author information is available at the end of the article

© The Author(s) 2026. **Open Access** This article is licensed under a Creative Commons Attribution 4.0 International License, which permits use, sharing, adaptation, distribution and reproduction in any medium or format, as long as you give appropriate credit to the original author(s) and the source, provide a link to the Creative Commons licence, and indicate if changes were made. The images or other third party material in this article are included in the article's Creative Commons licence, unless indicated otherwise in a credit line to the material. If material is not included in the article's Creative Commons licence and your intended use is not permitted by statutory regulation or exceeds the permitted use, you will need to obtain permission directly from the copyright holder. To view a copy of this licence, visit http://creativecommons.org/licenses/by/4.0/.

Springer

Keywords Chinese medicine residue, Biochar, Heavy metals, Solution, Soil, Resource recovery

Graphical Abstract



1 Introduction

The current global concern surrounding the issue of HM pollution of the environment, particularly in the form of wastewater and soil contamination, can be attributed to the persistence and toxicity of these substances. Statistical evidence indicates that HMs have contaminated 40% of the world's rivers and lakes (Zhou et al. 2020). Concurrently, approximately 2.3 billion individuals residing in disparate global regions are afflicted with waterborne illnesses due to the consumption of contaminated water, and the majority of these cases are from developing countries (Wang and Yang 2016). Industrial wastewater is a significant source of soil contamination, which presents a considerable risk to human health. It is estimated that 9 million people died prematurely from diseases associated with pollution in 2015, accounting for 16% of all global deaths (Landrigan et al. 2018). Soil contamination exceeds 16.1% of the threshold, while HMs exceed 1.1% (Cr), 7.0% (Cd), 2.7% (As), 1.5% (Pb) and 1.6% (Hg) respectively (Zhao et al. 2022). Plants absorb toxic metals from the soil during their growth process, and these metals may accumulate in the human body through the food chain, potentially causing serious human health problems. *Ligusticum chuanxiong* is one of the most widely used traditional Chinese medicines in China, with a range of applications in the treatment of various diseases, including cardiovascular and cerebrovascular diseases, neurodegenerative disorders, and psoriasis (Kong et al. 2024). However, due to the high cadmium content in the soil of the *Chuanxiong* cultivation area, coupled with its tendency to enrich heavy metals, it has been identified as one of the Chinese herbal medicines with serious heavy metal exceedance (Xie et al. 2023; Zhao et al. 2014). The remediation of wastewater and soil contaminated with HMs has emerged as a significant environmental challenge that requires immediate attention.

How to solve the contamination of soil and wastewater by HMs represents a significant environmental challenge, given the detrimental impact of these pollutants on ecological systems and human health. In the case of wastewater, the most commonly employed methods of HM treatment include chemical precipitation, ion exchange, membrane separation, electrochemical processes, adsorption, and biological methods (Abdullayev et al. 2024; Ayach et al. 2024; Ullah & Rahman 2024). Soil remediation techniques typically include physical, chemical, and biological remediation methods (Li et al. 2024; Nguyen et al. 2023). Among the aforementioned methods, the chemical adsorption method, exemplified by biochar, is characterized by low cost, high efficiency and minimal technical requirements (Aziz 2024; Bilias et al. 2023). In particular, biochar modified through chemical modification exhibits a more extensive specific surface area and a greater number of surface functional groups, thereby demonstrating superior performance in HM adsorption (Subramanian et al. 2024). The catalytic effect of potassium ions and phosphate on biochar adsorption of HMs has been demonstrated (Ahmad et al. 2018). Potassium is one of the essential elements indispensable for plant growth, as evidenced by the use of slow-release potassium fertilizer under drip irrigation to promote plant growth (Qu et al. 2024). Consequently, the development of potassium phosphate-modified multi-functional biochar with high selectivity, large adsorption capacity, high detection sensitivity and good stability, based on the traditional adsorption method, has the potential to reduce treatment costs, improve treatment efficiency and offer a promising practical application prospect.

This study focuses on the urgent environmental problem of lead and cadmium heavy metal pollution. In recent years, heavy metal pollution incidents have occurred frequently in China, seriously affecting people's lives and health, and the treatment of heavy metal-polluted wastewater and soil has become a prominent environmental problem that needs to be urgently addressed. The prepared phosphate-modified pharmaceutical residue biochar provides an effective solution for effectively sequestering heavy metals Pb and Cd in wastewater and soil. This study provides a simple and feasible solution for remediating Pb- and Cd-contaminated water and soil, while achieving agricultural waste recycling, thereby serving dual purposes with a single approach.

Traditional Chinese medicinal herb residues (TCMHR) are rich in resources, with high carbon content and organic components such as cellulose, hemicellulose, and lignin, making them an ideal raw material for preparing biochar. Our research group's previous studies have found that biochar derived from TCMHR and its modified composite materials show great potential in adsorbing heavy metal pollutants (Wang et al. 2024b; Yuan et al. 2024). However, the above studies have not been applied to the remediation of soil heavy metal pollution, and the effects of modified materials on plant growth have not been determined, which also limits the application space of the developed materials. In this study, phosphate-loaded biochar was successfully prepared and employed for the immobilisation of Cd/Pb in aqueous solution and contaminated soil. The objective of this study is threefold: firstly, to examine the adsorption capacity and mechanism of phosphate-loaded biochar on Cd/Pb; secondly, to assess the ecological risk of phosphorus-modified biochar in the remediation of heavy metals (Cd and Pb) in contaminated soil; and thirdly, to investigate the effect of materials on plant growth using pot experiments with *Ligusticum chuanxiong* as an example plant.

2 Materials and methods

2.1 Preparation of biochar and phosphorus-modified biochar

The chemicals and consumables used in the experiment are shown in Supporting Information Text S1.1. The residual materials of *Salvia miltiorrhiza* Bunge were selected as the raw materials and obtained from Xinfuyuan Chinese Herbal Pieces Co. Ltd. The original biochar was prepared by placing the dregs of *Salvia miltiorrhiza* (particle size < 2 mm) into a tube furnace and heating them to 600 ℃ at a rate of 10 °C min^{-1} under oxygen-limited conditions for two hours. This product is referred to as BC. The method for the preparation of phosphorus-modified biochar was determined on the basis of previously reported methods (Yang et al. 2021; Yuan et al. 2024; Zhang et al. 2020b). Further discussion of this method can be found in Supporting Information Text S1.2 and Text S1.3. The determination of the physical and chemical properties of biochar can be found in Supporting Information Text S1.4.

2.2 Evaluation of Pb/Cd adsorption on modified biochar

The screening test of initial pH on the adsorption of Pb/Cd by modified biochar is shown in Supporting Information Text S1.5. Batch adsorption experiments were conducted to investigate the adsorption properties of modified biochar for Pb and Cd. The adsorption kinetics were initially investigated through the following methodology: 10 mg of modified biochar was combined with 25 mL of a 0.01 mol L^{-1} $NaNO_3$ solution in a 50 mL centrifuge tube, which contained a 300 mg L^{-1} $Pb(NO_3)_2$ solution or a 50 mg L^{-1} $Cd(NO_3)_2$ solution. The optimal pH value for adsorption was adjusted by the addition of a small quantity of 1 M HNO_3 or NaOH solution. The centrifuge tube was placed in a constant-temperature shaker set at 25 ℃

and oscillated at 220 rpm. Additionally, samples were collected at 0–60 h and filtered through a 0.45 μm microporous membrane. The concentration of Pb and Cd in the filtrate was determined using ICP-OES, and the adsorption amounts of Pb and Cd by biochar at different times were obtained. The results were fitted by five kinetic models: the pseudo-first-order, pseudo-second-order, intra-particle diffusion, Elovich and Bangham models.

In the adsorption isotherm experiment, the Pb concentration was set within the range of 200–1000 mg L^{-1}, with gradients of 200, 300, 400, 600, 800 and 1000 mg L^{-1}, respectively. The concentration of Cd was set within the range of 5–50 mg L^{-1}, with gradients of 5, 10, 15, 25, 35 and 50 mg L^{-1}, respectively. The remaining steps were conducted in accordance with the procedures established for the kinetic experiment, and the results of the adsorption isotherm experiment were obtained. The results were fitted using the Langmuir, Freundlich and Sips isotherm models.

The adsorption capacity (Q, mg g^{-1}) of the adsorbent was calculated using the formula (1):

$$Q = (C_o - C_t) \times \frac{v}{m} \quad (1)$$

where, C_o and C_t are the initial and equilibrium heavy metal concentrations (mg L^{-1}), respectively, v is the volume of the solution (L), and m is the mass of the added biochar (g).

In order to study the mechanism of Cd/Pb removal by phosphate-loaded biochar, the characteristics of 3K-BC before and after adsorption of HMs were analyzed. For the biochar adsorbed in solution, we obtained the material by centrifugal separation. Scanning electron microscopy combined with energy dispersive spectrometer (SEM–EDS, ZEISS Axio Imager M2 EVO10, Germany) was used to observe the surface morphology images of biochar samples before and after adsorption. X-ray diffraction (XRD, Rigaku Ultma IV, Japan) was used to analyze the crystallization characteristics of the samples. Fourier transform infrared spectroscopy (FT-IR, PerkinElmer Frontier, China) was used to qualitatively analyze the surface functional groups of biochar in the wavenumber range of 400–4000 cm^{-1}. X-ray photoelectron spectroscopy (XPS, Thermo Scientific K-Alpha, USA) was used to obtain the surface element composition and the relative percentage of the surface elements.

2.3 Preparation and incubation of contaminated soil samples

The experimental soil was sampled from Pengzhou City, Sichuan Province, which is a region renowned for the production of Chinese medicinal materials, namely *Chuanxiong*. The methods outlined in Supporting Information Text S1.6 detail both the collection procedure and the determination techniques for the fundamental physical and chemical properties of the sample soil.

The standard solution of Cd and Pb, procured from the Henan R&D Center for Certified Reference Materials, was introduced to the soil. The soil was cultivated for 50 days under conditions of saturated water holding capacity of 45% at room temperature, resulting in the formation of a mixed contaminated soil with high and low concentrations of standard HMs (Li et al. 2022a; Xia et al. 2021). To assess the adsorption of HMs in contaminated soil by modified biochar, incubation experiments were conducted in 500 mL plastic conical flasks. The modified biochar was incorporated into the contaminated soil samples at two different doses (1% and 3%) in order to assess its efficacy. The soil samples were mixed with the biochar until a homogeneous mixture was achieved. The experimental groups are shown in Table 1. Each treatment was conducted in triplicate. Subsequently, the soil samples were incubated at room temperature with constant humidity (45% water holding capacity) for 60 days (Wang et al. 2021). According to the Soil Environmental Quality Risk Control Standard for Soil Contamination of Agricultural Land (GB15618-2018), the low HM concentration is defined as 200 mg kg^{-1} Pb and 0.5 mg kg^{-1} Cd. The term "high heavy metal concentration" is used to describe a composition of 500 mg kg^{-1} of Pb and 3 mg kg^{-1} of Cd. Following the incubation period, the soil samples were air-dried, and approximately 100 g of soil was ground and passed through 2 and 0.15 mm sieves and stored for subsequent physical and chemical analyses. To facilitate a more detailed examination of the adsorption processes between materials and HMs, the group 6 was selected as a case study. Then, the adsorbed material was collected by using a sieve and tweezers for further characterization analysis. The adsorbed biochar was analyzed using a combination of techniques, including SEM–EDS, XRD, FT-IR, and XPS.

This process encompasses acid, neutral, and alkaline phosphatase (Zhang et al. 2023b). The neutral phosphatase of soil was determined by citrate

Table 1 Grouping conditions in soil experiments

Grouping category	Soil treatment	Abbreviation
Control	Blank soil	CK
Group 1	Low HMs + 0% 3K-BC	LHM0
Group 2	Low HMs + 1% 3K-BC	LHM1
Group 3	Low HMs + 3% 3K-BC	LHM3
Group 4	High HMs + 0% 3K-BC	HHM0
Group 5	High HMs + 1% 3K-BC	HHM1
Group 6	High HMs + 3% 3K-BC	HHM3

Low heavy metal concentrations are those consisting of 200 mg kg^{-1} Pb and 0.5 mg kg^{-1} Cd, and high heavy metal concentrations are those consisting of 500 mg kg^{-1} Pb and 3 mg kg^{-1} Cd

buffer-colorimetry, in accordance with the neutral pH of the soil (Chen et al. 2024b). The determination of urease was conducted using sodium phenol-sodium hypochlorite colorimetry (Zhao et al. 2021). The effective phosphorus content of the various groups was determined by sodium bicarbonate extraction-molybdenum-antimony spectrophotometry, in accordance with the "substitution" of phosphorus fertilisers for phosphorus-modified biological carbon (Li et al. 2020). Additionally, the sustained-release impact of the experimental materials on phosphorus was assessed through the effective phosphorus content extracted through repeated leaching. In order to investigate the impact of the materials on soil water-holding capacity, experiments were conducted to assess their water-holding capacity (Lu et al. 2023). The specific methodology is as follows: One gram of BC/3K-BC was combined with 150 g of dry soil, 50 mL of ultrapure water was added, and the mixture was weighed after blending (W_0). The samples were stored at room temperature and weighed at regular intervals. The formula was as follows:

$$WR\% = \left(\frac{m_t}{m_0}\right) \times 100\% \tag{2}$$

2.4 Speciation analysis of heavy metals in soil

The sequential extraction procedure developed by the European Community Bureau of Reference (BCR) was employed to examine the concentration of Cd and Pb in the amended soil (Li et al. 2022a, 2022c). In summary, 1.00 g of a biochar-soil mixture was transferred to a 50 mL polytetrafluoroethylene tube. The acid-soluble, reducible, oxidizable, and residual components of HM_S were obtained through extraction. The following solutions were prepared: 0.11 M acetic acid (40 mL), 0.5 M $NH_2OH{\cdot}HCl$ (40 mL, pH = 2), 8.8 M H_2O_2 (10 mL, pH = 2), 1 M NH_4OAc (20 mL, pH = 2), and aqua regia (HCl/HNO_3, 3:1, 8 mL), respectively. The concentration of HMs in each component was determined by inductively coupled plasma optical emission spectrometry (ICP-OES).

2.5 Bioavailability and potential ecological risk assessment

The bioavailability of HMs to soil organisms was analyzed using the $CaCl_2$ extraction method (Xia et al. 2020), as this has been demonstrated to be an effective indicator for assessing plant availability (Gu et al. 2020; Yin et al. 2016). In summary, the soil was extracted with 0.01 M $CaCl_2$ at 20 ℃ for two hours using a soil extraction ratio of 1:5 (w/v). The mixture was then subjected to shaking and centrifugation at 3000 rpm for a period of 15 min. Subsequently, the supernatant was filtered through a 0.45 μm microporous membrane, and the concentration of Pb and Cd in the extract was determined by ICP-OES.

The Toxicity Characteristic Leaching Procedure (TCLP) was employed to evaluate alterations in leaching toxicity in enhanced soils (Chaudhary and Rao 2024). In general, a soil sample of 5 g was mixed with 100 mL of a 0.5 M glacial acetic acid solution with a pH of 2.88. Following a period of continuous oscillation lasting 16 h, the supernatant was obtained by means of centrifugation. The samples were prepared using a 0.45 μm microporous membrane, and the concentrations of Cd and Pb were subsequently analyzed using ICP-OES. All tests were conducted in triplicate. In this study, the Nemerow index and the Potential Ecological Risk index were employed for the assessment of the ecological risk associated with the presence of HMs in soil (Hakanson 1980). The Nemerow index is calculated as follows:

$$P_i = \frac{C_i}{S_i} \tag{3}$$

$$NPI = \sqrt{\frac{{P_{max}}^2 + {P_{avr}}^2}{2}} \tag{4}$$

where P_i is the single pollution index, C_i is the extraction concentration of heavy metals by TCLP in the soil after the pot experiment, S_i is the TCLP international standard (the concentrations of Pb and Cd are 5 and 0.5 mg kg^{-1}, respectively), NPI is the Nemerow comprehensive pollution index, P_{max} is the maximum value of the pollution index, and P_{avr} is the average value of the single pollution index.

The potential risk index is calculated as follows:

$$E_i = T_i \times P_i \tag{5}$$

$$PI = \sum_{i=1}^{n} E_i \tag{6}$$

where E_i is the single potential ecological risk index; T_i is the toxic reaction coefficient of a single heavy metal (Pb is 5, Cd is 30), and P_i is a single pollution index. PI is the comprehensive potential ecological risk index of polymetallic.

2.6 Pot experiment of *Ligusticum chuanxiang*

The objective of this study was to utilize *Ligusticum chuanxiang*, cultivated in pots, as a material for experimental design in order to investigate the impact of plant growth. Before the experiment, the contents of heavy metals Pb and Cd in the soil were measured as described in Supporting Information Text S1.6. The soil was prepared for contamination by the addition of a standard solution of HMs (Nigam et al. 2021). The Pb concentration was set at 200 mg kg^{-1}, while the Cd concentration was set at 3 mg kg^{-1}. The experimental design was

divided into the following groups: BK (normal soil), 1% BC-BK (1% 3K-BC + normal soil, 1%, w/w), 0% BC-HM (0% 3K-BC + contaminated soil) and 1% BC-HM (1% 3K-BC + contaminated soil). A total of four groups were established, with each group comprising six replicates. Following a seven-month cultivation period in a natural environment, the roots, stems and leaves of *Ligusticum chuanxiong* were harvested and washed with deionised water. The primary indices for evaluating the *Ligusticum chuanxiong* include yield, distribution of HMs, and the content of active ingredients. The distribution of HMs in different plant parts was determined by microwave digestion (Table S1) and ICP-MS. The medicinal ingredients, including ferulic acid, ligustilide A and ligustilide, were analyzed by high-performance liquid chromatography (HPLC, Agilent 1260, USA) and a chromatographic column (Thermo BDS C_{18}, 4.6 mm × 250 mm, 5 μm) (Han et al. 2023).

The bioconcentration factor (*BCF*) and transfer factor (*TF*) are calculated as:

$$BCF = \frac{M_{plant}}{M_{soil}} \tag{7}$$

$$TF = \frac{M_{abovegroud}}{M_{root}} \tag{8}$$

where M_{plant} is the Pb/Cd concentration in plant biomass, and M_{soil} is the total concentration of HMs in soil, in mg kg^{-1}. $M_{aboveground}$ is the concentration of HMs in the aboveground part of the plant tissue, while M_{root} is the concentration of HMs in the root.

2.7 Statistical analysis

Differences between experimental groups were compared by one-way analysis of variance and expressed as the least significant difference. A p-value of <0.05 was considered to be statistically significant. Each treatment was repeated three times, and the results are shown as the mean values. The simple data analysis part was executed by Microsoft Office Excel 2016. Data fitting and some characterization results were completed with the assistance of Origin 2021.

3 Results and discussion

3.1 Adsorption characteristics of Pb and Cd in solution

3.1.1 Adsorption dynamics

In order to gain further insight into the adsorption mechanism and rate-limiting steps, five kinetic models were employed to fit the data, namely the pseudo-first-order model, the pseudo-second-order model, the intraparticle diffusion model, the Elovich model and the Bangham model. The results of the experimental investigation into the kinetics of Pb and Cd adsorption on 3K-BC are presented in Fig. 1 and Table 2. In general, 3K-BC achieved equilibrium adsorption of Pb within approximately 600 min. At approximately 400 min, 3K-BC achieved equilibrium for Cd adsorption. This indicated that Cd was adsorbed at a faster rate than Pb. The R^2 values of the pseudo-second-order kinetic model for Pb and Cd were higher, at 0.9926 and 0.9606, respectively, than those of the pseudo-first-order kinetic fitting parameters. The equilibrium adsorption capacities of 128.95 mg g^{-1} (Cd) and 352.73 mg g^{-1} (Pb), as fitted by the pseudo-second-order model, were found to be in closer alignment with the value of the experimental adsorption capacity. Therefore, the adsorption process in this experiment is best described by the pseudo-second-order kinetic model, indicating that chemical adsorption is the primary mechanism and that the number of active sites on the material's surface controls the adsorption rate of Pb and Cd on 3K-BC (Li et al. 2023).

The intraparticle diffusion model was used to describe heterogeneous adsorbent diffusion. As illustrated in Fig. 1D and Table S2, three distinct phases can be discerned in the Pb adsorption process on 3K-BC: external diffusion, internal diffusion, and adsorption equilibrium (Sun et al. 2022; Zhou et al. 2023). Initially, Pb diffused from the solution to the outer surface of the adsorbent. This was predominantly due to the interaction between the HMs and the electrostatic attraction present on the adsorbent's surface. The second stage was designated as intraparticle diffusion, during which HMs from the adsorbent's outer surface entered the active sites within the pores and bonded with them, thereby functioning as an adsorbent. Subsequently, the rate of adsorption declined until it reached equilibrium. The Pb data were consistent with the intraparticle diffusion model, as indicated by the R^2 values for each step. Moreover, the third R^2 value for Cd was 0.672, indicating that the adsorption process of Cd consisted of only two stages. Concurrently, the diffusion rate constants for each stage exhibited a progressive decline ($K_1 > K_2 > K_3$), indicating that the reaction was slowing down and that the final rate was approaching zero, suggesting that the adsorption capacity was no longer changing over time. Figure 1D demonstrated that the removal of the two heavy metals was multi-linearly correlated, with the intercepts of the fitting lines C_1, C_2 and C_3 not equal to zero. This indicates that internal diffusion was not the sole rate-limiting step in controlling the removal of HMs, and that the adsorption rate should be influenced by both external diffusion and internal diffusion (Li et al. 2023; Yilmaz and Guzel 2021).

The Elovich kinetic model, which is widely applied in many different contexts, particularly to the removal of pollutants from aqueous solutions, describes the

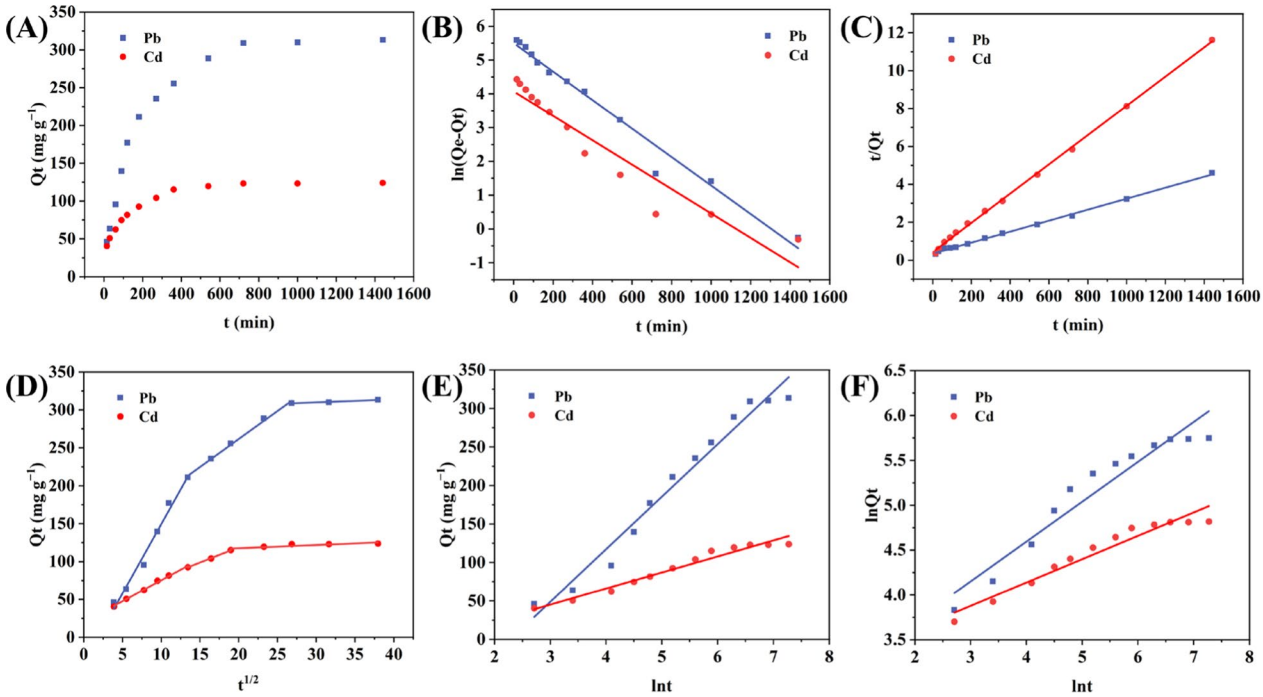


Fig. 1 3K-BC adsorption kinetics of Pb and Cd (**A**) and different kinetic fitting models: (**B**) pseudo-first-order model; (**C**) pseudo-second-order model; (**D**) intraparticle diffusion model; (**E**) Elovich model; (**F**) Bangham model

Table 2 Fitting parameters of adsorption kinetics model of Pb and Cd by 3K-BC

Kinetic model	Parameter	Pb	Cd
Pseudo-first-order kinetic model	Q_e (mg g^{-1})	304.15	117.81
	K_1	0.0065	0.0119
	R^2	0.9851	0.8831
Pseudo-second-order kinetic model	Q_e (mg g^{-1})	352.73	128.95
	K_2	0.000022	0.00014
	R^2	0.9926	0.9606
Intraparticle diffusion model	Kip	8.3821	2.5215
	R^2	0.8359	0.8003
Elovich model	A	4.8884	8.1232
	B	0.0131	0.0468
	R^2	0.9640	0.9622
Bangham diffusion model	M	2.2510	3.8388
	K_b	16.7450	22.1203
	R^2	0.9192	0.9400

speed of substance diffusion and propagation in the medium (Bukhari et al. 2024). Table 2 presents the correlation coefficients R^2 for Pb and Cd, which were both greater than 0.95. These values indicated that the model was consistent with the 3K-BC adsorption process for the two heavy metals (Hu et al. 2020; Liu et al. 2020), which involved both heterogeneous diffusion and a chemical reaction. The pore diffusion model is frequently described by the Bangham model. The linear diagram for the Bangham pore diffusion model is presented in Fig. 1F. The correlation coefficient R^2 values for Pb and Cd were 0.9192 and 0.9400, respectively. This indicated that pore diffusion occurred during the adsorption process, but that other factors also affected the adsorption rate (Berslin et al. 2022).

3.1.2 Adsorption isotherm

The dependence curve between the concentration of pollutants in the liquid phase and their amount adsorbed on the solid phase is referred to as the adsorption isotherm. The Pb and Cd adsorption isotherms on 3K-BC are illustrated in Fig. 2. The data pertaining to the adsorption isotherms of the two HMs under investigation exhibited an L-shaped pattern, initially demonstrating an upward trajectory before reaching a point of stabilisation. In other words, as the equilibrium concentration increased, the modified biochar exhibited an enhanced adsorption capacity for HMs, reaching a state of saturation. However, 3K-BC exhibited a markedly higher adsorption capacity for Pb than for Cd. The experimental results pertaining to the adsorption isotherms were subjected to analysis using the Langmuir, Freundlich, and Sips models with a view to investigating the adsorption process of biochar on HMs. The fitting results are

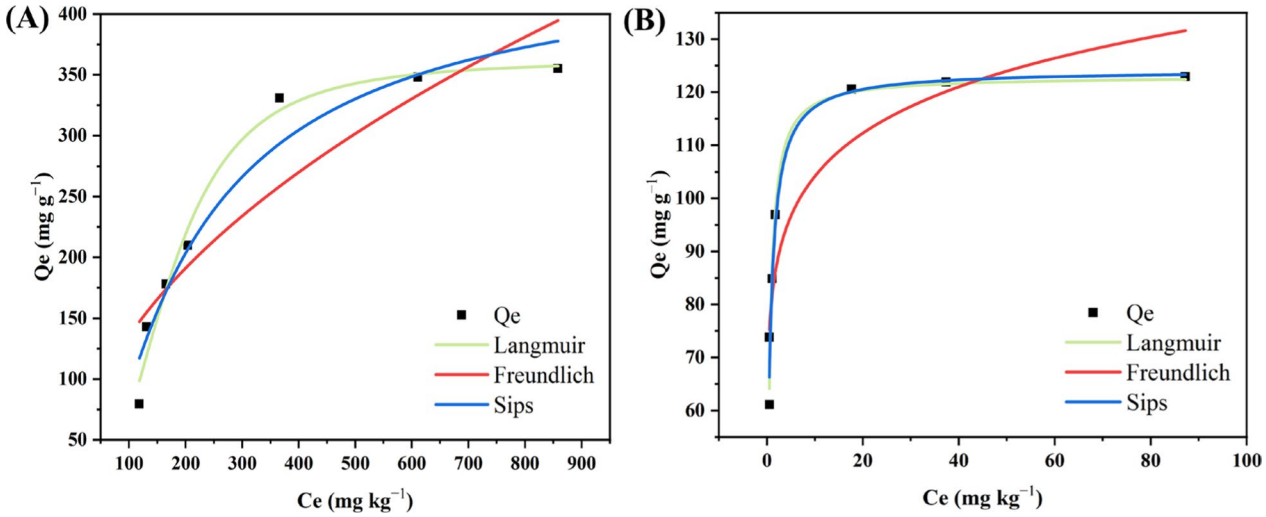


Fig. 2 Adsorption isotherms of Pb (**A**) and Cd (**B**) on 3K-BC

presented in Table S3. The data in the table indicate that the adsorption process of Pb and Cd by 3K-BC was more accurately represented by the Langmuir model than by the Freundlich model, with correlation coefficients R^2 of 0.9743 and 0.9516, respectively. This indicated that Pb and Cd were adsorbed onto the material via a monolayer adsorption process. From the Langmuir model fit, the maximum adsorption capacities of 3K-BC for Pb and Cd were determined to be 361.82 mg g^{-1} and 123.03 mg g^{-1}, respectively. According to the Freundlich model, the constant 1/n for the two HMs was less than 0.5, indicating that 3K-BC exhibited a pronounced adsorption effect on Pb and Cd and that the adsorption procedure was straightforward (Wang et al. 2018). The Sips isotherm model is considered a hybrid of the Freundlich and Langmuir models, offering a solution to the limitations of both. The Sips isotherm model indicated that the fitting parameters R^2 for Pb and Cd were less than 0.95, at 0.9287 and 0.9473, respectively. Concurrently, the actual Pb adsorption capacity (355.15 mg g^{-1}) differed considerably from the theoretical maximum Pb adsorption capacity by 3K-BC (456.38 mg g^{-1}). Therefore, the Sips isotherm model is unsuitable for elucidating the mechanism of Pb adsorption by this experimental material.

Table 3 presents the maximum theoretical adsorption capacity of modified biochar for the removal of Pb or Cd, as reported in the literature. In contrast, the experimental material demonstrated a higher Pb and Cd adsorption capacity than that observed in the majority of previously reported biochars. The research results show that the 3K-BC prepared in this study has significant potential for removing the two heavy metals, Pb and Cd.

3.1.3 Potential adsorption mechanism in solution

The SEM–EDS results of the biochar are shown in Fig. S1 and Fig. 3. The surface of the pristine biochar exhibited a rough and porous structure. Following modification, no notable alterations were observed in the surface. Given its porous structure, it is hypothesised that the surface is capable of physically adsorbing HMs. The semi-quantitative results obtained by EDS demonstrated that the potassium content increased from 4.21% to 18.85%, and the phosphorus content increased from 0.24% to 3.63% following the modification with potassium phosphate. This indicated that the modification with potassium phosphate was indeed successful. Following the adsorption of both HMs, the presence of precipitated compounds on their surfaces was observed, particularly after Pb adsorption. The phenomenon of particles on the surfaces was more pronounced. The semi-quantitative results of EDS after adsorption demonstrated a notable decline in the content of both elemental K and P on the surface of modified biochar, whereas the content of HMs Pb and Cd exhibited a marked increase. These findings substantiate the pivotal role of potassium and phosphorus elements in the adsorption of HMs. The underlying mechanisms involved are postulated to encompass precipitation between phosphate and heavy metal ions, as well as cation exchange involving potassium ions (Lin et al. 2023).

The distinct surface functional groups of the four biochars were identified through FT-IR spectroscopy within the wavelength range of 400–4000 cm^{-1}, as illustrated in Fig. 4A. The wave number at 1689 cm^{-1} prior to ads orption was observed to shift to 1658 cm^{-1} following adsorption. This shift was attributed to the vibration of the C=O

Table 3 Adsorption characteristics of Pb and Cd removal by different phosphorus modified biochars

Biochar type	Contaminant	Pyrolysis condition	Kinetic model	Isotherm model	Adsorption capacity (mg g^{-1})	Reference
Reed straws	Pb	400 ℃, 2 h	–	Langmuir	59.3	Cui et al. (2022)
Tree branches	Cd	500 ℃, 2 h	Sec	Langmuir	116	Wang et al. (2022)
Chicken feather	Pb	450 ℃, 1 h	Sec	Freundlich	55.43	Chen et al. (2019)
	Cd	450 ℃, 1 h	Sec	Langmuir	7.84	
Sawdust	Pb	500 ℃, 1/3 h	Sec	Langmuir	48.5	Yang et al. (2023)
	Cd		Sec	Langmuir	13.6	
Peanut shell	Pb	500 ℃, 1/3 h	Sec	Langmuir	82.3	Yang et al. (2023)
	Cd		Sec	Langmuir	41.5	
Rape straw	Cd	600 ℃, 1 h	Sec	Langmuir	81.80	Li et al. (2017)
Corn stalks	Pb	800 ℃, 2 h	Sec	Langmuir	357.76	Li et al. (2022b)
Peanut shells	Cd	500 ℃, 2 h	Sec	Langmuir	138	Huang et al. (2022)
Medicine residues	Pb	500 ℃, 3/4 h	Sec	Langmuir	599.4	Chen et al. (2022)
Grape pomace	Pb	500 ℃, 2 h	Sec	Langmuir	134	Jin et al. (2020)
Nutshell	Pb	500 ℃, 2 h	Sec	Freundlich	79.26	Wang et al. (2024a)
3K-BC	Pb	600 ℃, 2 h	Sec	Langmuir	361.82	This study
	Cd	600 ℃, 2 h	Sec	Langmuir	123.03	

group (Gao et al. 2019, 2020). It was postulated that at this juncture, the C=O functional group participated in the precipitation of the metal ions, which resulted in the aforementioned shift in the wavenumber. The peak at 1575 cm^{-1} was attributed to –COOH (Wang et al. 2022), and the peak at 1390 cm^{-1} is attributed to the stretching vibration of CO_3^{2-} (Yang et al. 2023). The peak at 874 cm^{-1} is attributed to the out-of-plane bending vibrational absorption peaks of C–H bonds. Furthermore, the modified biochar exhibited a peak at 1043 cm^{-1}, attributed to PO_4^{3-}, confirming the successful loading of phosphate ions (Zhou et al. 2022). This finding is in accordance with the results obtained from the scanning electron microscope with energy-dispersive X-ray spectroscopy. A comparison with BC before modification revealed that the IR spectra of 3K-BC exhibited a greater number of peaks, thereby demonstrating that the modified material possessed a greater number of functional groups on its surface. The reduction in the intensity of the PO_4^{3-} peak or the shift in the peak position following the adsorption of HMs indicated that phosphorus-containing functional groups were involved in the interactions with HMs. Similar observations were made with regard to other functional groups. In conclusion, the diverse array of oxygen-containing functional groups present on the biochar surface may prove instrumental in the adsorption and immobilisation of heavy metals (Zong et al. 2021).

The XPS spectra for the pre- and post-adsorption states are presented in Fig. 4B–G. The full spectrum demonstrates that following the adsorption of Pb on the biochar, new peaks corresponding to Pb 4f were observed at 138.32 and 143.05 eV. Similarly, the adsorption of Cd onto the biochar resulted in the emergence of new peaks belonging to Cd 3d at 405.72 and 412.04 eV. This suggests that both HMs were successfully adsorbed onto the 3K-BC surface. Figure 4C depicts the C 1s spectrum of the biochar. Following modification, the peaks at binding energies 284.75 (61.65%), 285.60 (36.34%) and 289.43 eV (2.00%) were found to correspond to C–C/C–H, C–O/C–N and COOH functional groups (Das et al. 2023). Following the adsorption of Pb/Cd, the positions and peak intensities of the characteristic peaks of these groups underwent changes. The formation of Pb/Cd–O complexes with C–O can occur, which results in a reduction in the relative content of C–O (Huang et al. 2022). It is speculated that it is due to the precipitation or complexation with Pb/Cd, resulting in the loss or increase of groups (Li et al. 2022b).The aromatic structure of biochar has been demonstrated to facilitate ion exchange with HMs through the donation of π-electrons during the process of adsorption. This resulted in the formation of metal-π complexes (Harvey et al. 2011). Following the adsorption of Pb, the content of COOH increased from 2.00% to 10.42%, indicating the formation of Pb-COOH complexes. Conversely, after the adsorption of Cd, the content of COOH decreased, suggesting that the adsorption mechanism may involve ion exchange (Zhou et al. 2022). As illustrated in Fig. 4D, the three peaks observed in the O 1s fine spectrum of 3K-BC, located at 530.97 eV (24.90%), 531.94 eV (53.25%), and 533.47 eV (21.85%), were attributed to C=O/P=O, C–O/P–O, and

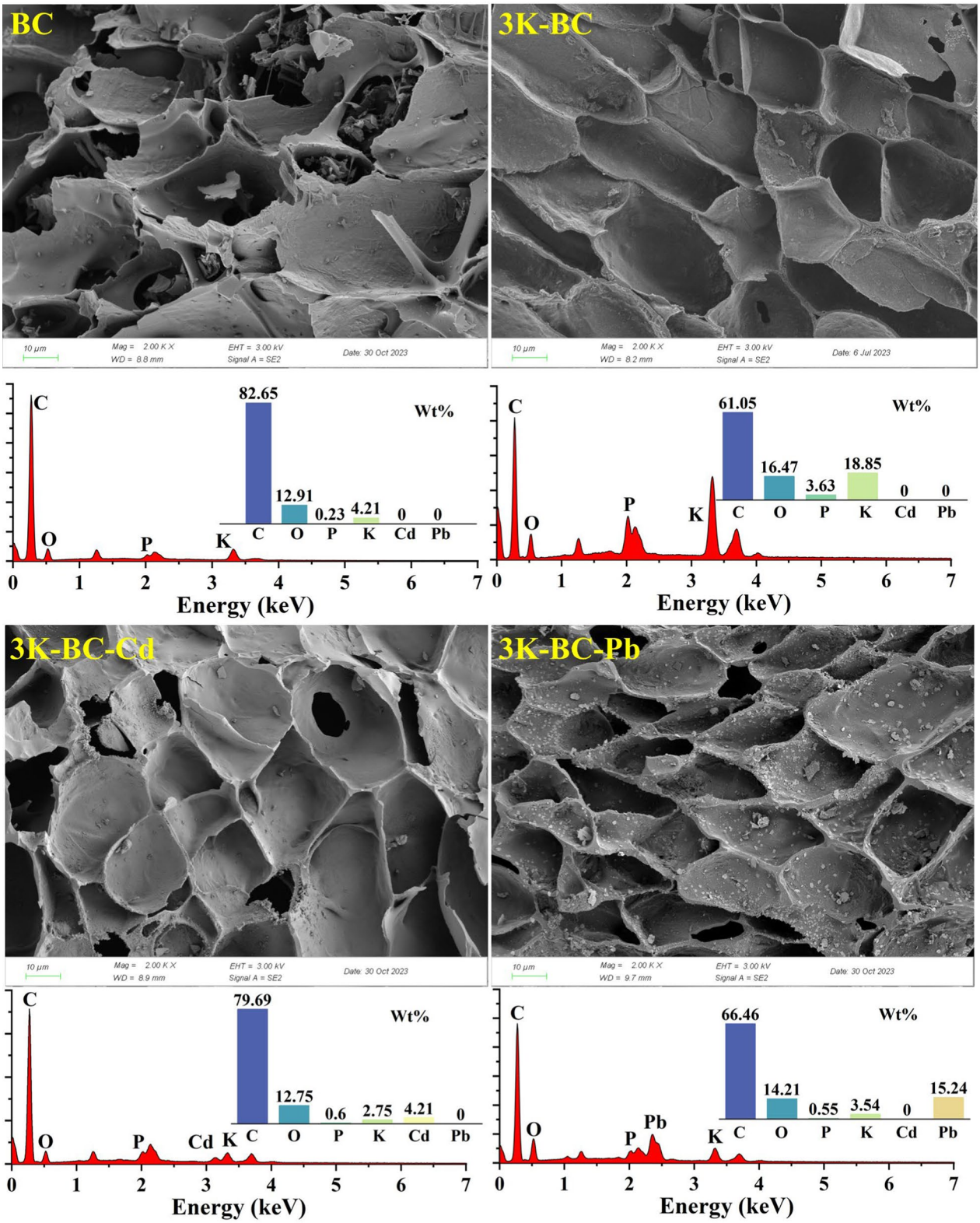


Fig. 3 SEM–EDS spectra of BC and modified biochar before and after adsorption of HMs

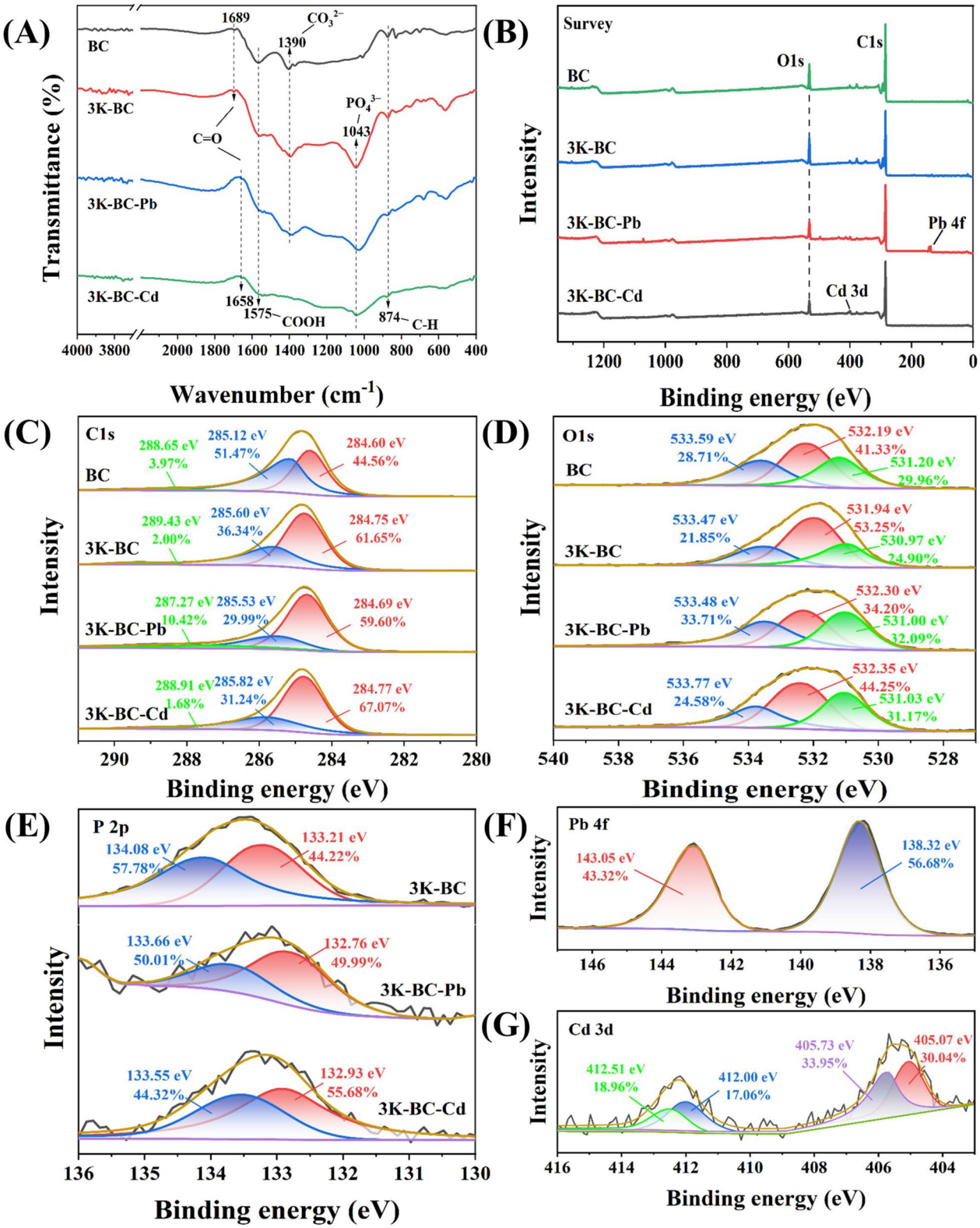


Fig. 4 **(A)** the FT-IR spectra of four biochars. The XPS spectra of the four biochars, including (**B**) survey, (**C**) C1s, (**D**) O1s, (**E**) P 2p, (**F**) Pb 4f, and (**G**) Cd 3d spectra

–OH/O–C=O groups, respectively (Herath et al. 2021; Zhou et al. 2022). Following the adsorption process, the percentage of C=O/P=O increased from 24.90% to 32.09% and 31.17%, respectively. This suggested the formation of $PbPO_4$ or $CdPO_4$ precipitates (Zhou et al. 2022). Additionally, other oxygen-containing functional groups had the potential to complex with HMs (Liu et al. 2024).

Following phosphate modification, peaks corresponding to P 2p were observed for 3K-BC, thereby confirming the successful loading of phosphate during the co-pyrolysis process. This finding was consistent with the SEM–EDS and FT-IR results. As illustrated in Fig. 4E, the peaks at 133.21 (44.22%) and 134.08 eV (57.78%) of 3K-BC correlated with P=O and P–O, respectively (Zhang et al. 2020b). Following the adsorption of Pb/Cd, the proportion of P=O increased to 49.99% and 55.68%, respectively, while the proportion of P–O groups decreased to 50.01% and 44.32%, respectively. This suggests that P=O and P–O are involved in the adsorption process (Lu et al. 2023). The peaks observed at 138.32 and 143.05 eV in Fig. 4F can be attributed to Pb $4f_{7/2}$ and Pb $4f_{5/2}$, respectively (Li et al. 2023). The difference of 4.8 eV between the two peaks was indicative of the presence of the Pb–O structure (Luo et al. 2019; Zhang et al. 2023a). The Pb $4f_{5/2}$ peak was associated with chemical states that were characterised by electrostatic attraction, porosity, or electronic interactions, whereas the Pb $4f_{7/2}$ peak was linked to chemical states that were associated with precipitation, ion exchange, or complexation (Wang et al. 2024a). The peak area of Pb $4f_{7/2}$ was found to be significantly larger than that of Pb $4f_{5/2}$, indicating that chemisorption played a dominant role in the adsorption process. The two peaks observed at 405.07 and 412.00 eV in Fig. 4G were attributed to Cd and the two peaks observed at 405.73 and 412.51 eV were attributed to Cd–O (Lin et al. 2023). Among these, Cd–O was adsorbed on the surface of the material as a precipitate through metal-π electron bonding (Behbahani et al. 2021).

The results, derived from ^{31}P NMR analysis, indicated that the surface of the phosphorus-modified biochar predominantly comprises orthophosphate composition (in Supporting Information Text S1.4.). Therefore, the main form of co-precipitation between P and Cd in the material may be considered to be Cd-orthophosphate, which is consistent with the findings of previous studies (Wang et al. 2022). The results indicated that the adsorption of Pb and Cd was facilitated by a combination of processes, including physical adsorption, precipitation, complexation of oxygen-containing functional groups, and cation exchange (Khalid et al. 2017; Li et al. 2023; Wu et al. 2021). The mechanism of adsorption is illustrated in Fig. S2.

3.2 Effects of soil properties

In order to investigate the impact of biochar supplementation on soil characteristics, the activities of enzymes, the availability of phosphorus and the capacity to retain water were examined. Enzyme activity is closely related to environmental conditions and can be used as an important biological index to detect soil changes, as well as evidence of heavy metal fixation in soil (Liao et al. 2023). In the regulation of soil ecosystems, urease plays a pivotal role in determining nitrogen flow (Song et al. 2022). Phosphatase plays a pivotal role in facilitating the conversion of organic phosphorus present in soil into inorganic phosphorus that can be absorbed and utilized by plants.

3.2.1 Enzyme activity assay

The contents of urease and phosphatase in soils with different rates of 3K-BC application are illustrated in Fig. 5A, B. Phosphatase and urease are hydrolytic enzymes. The activity of phosphatase was found to be positively correlated with total phosphorus, while urease was positively correlated with nitrogen. These correlations reflected the soil fertility level and the biotoxicity of HMs (Zhang et al. 2020a). In comparison to the control sample, the addition of high and low concentrations of HMs resulted in the inhibition of both enzymes. Furthermore, the inhibition effect was found to be more pronounced with increasing HM concentration. Following the application of 1% 3K-BC, a notable moderation in both enzyme activities was observed, with the urease and phosphatase content in the LHM1 group exceeding that of the CK group. This demonstrated the capacity of the material to stimulate the two enzymes, with the alkaline biochar potentially increasing urease and phosphatase contents by directly modifying the pH of the acidic soil (Song et al. 2022). Additionally, the active materials released by BC in the soil have been demonstrated to enhance the activities of urease and phosphatase (Wang et al. 2020). Upon increasing the application rate 3%, both LHM3 and HHM3 exhibited comparatively weak promotion of urease activity in comparison to the control group without 3K-BC. Conversely, 3% of 3K-BC demonstrated inhibition with regard to phosphatase. It can therefore be concluded that the material at a 1% application rate was more effective for soil enzyme activity. It is not recommended that the dose be increased to 3%.

3.2.2 Effective phosphorus content

The effective phosphorus content of 3K-BC for different treatment groups is shown in Fig. 5C. The effective phosphorus content demonstrated an increase in line with the rise in biochar application rate. The effective phosphorus

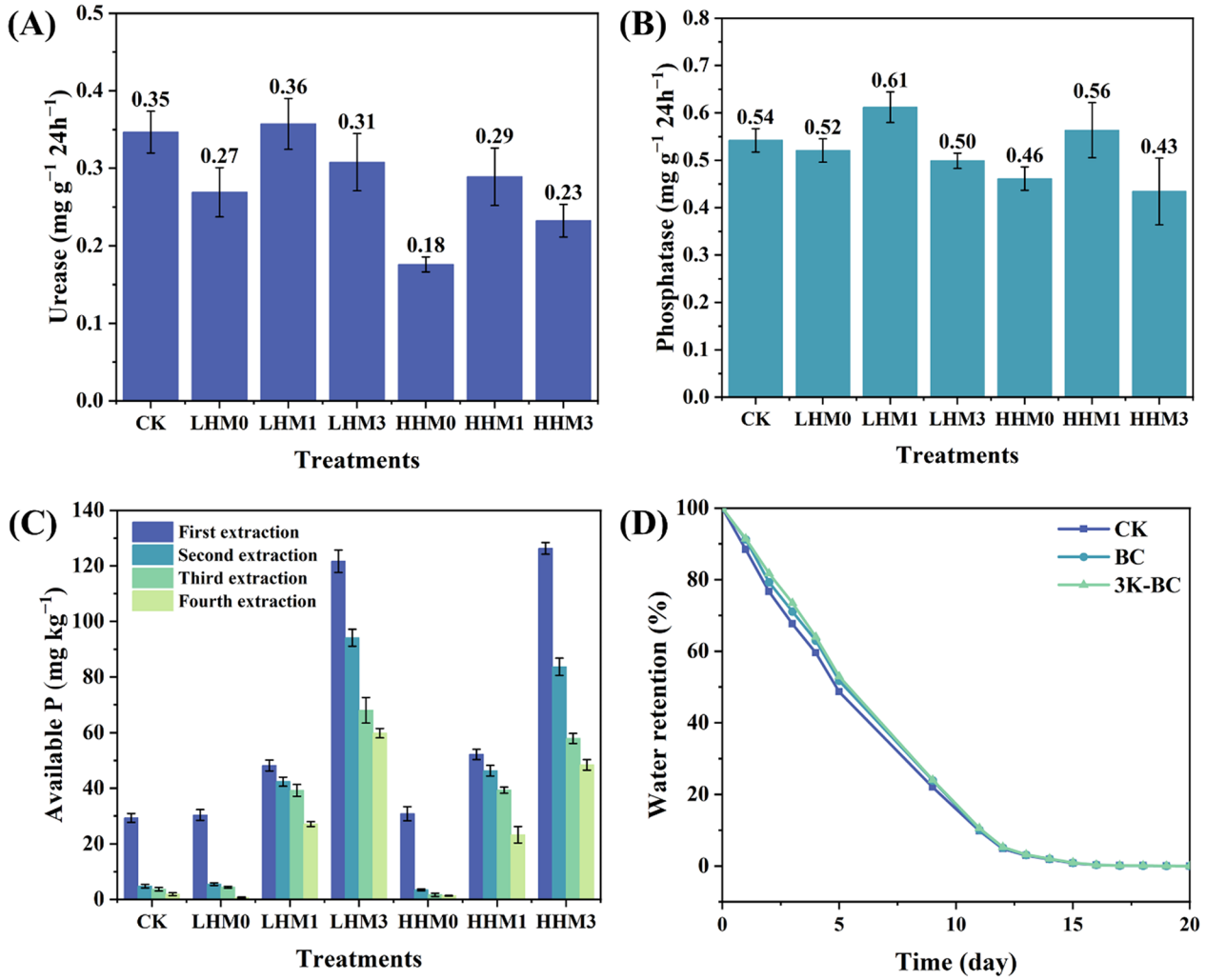


Fig. 5 The contents of urease (**A**) and neutral phosphatase (**B**) of 3K-BC after incubation in soil; (**C**) the content of multiple available phosphorus extracted by 3K-BC in soil; (**D**) the effect of adding different biochars on soil water retention

content of all three groups (CK, LHM0, and HHM0) was undetectable at the conclusion of the initial extraction period. For LHM1 and HHM1 with an application rate of 1%, the remaining effective phosphorus content after four extractions was 56% and 45% of the initial value, respectively. A comparable phenomenon was observed in the group with an application rate of 3%. This suggested that the materials had a gradual release effect on the release of effective phosphorus, which was in accordance with the findings reported in the literature (Li et al. 2020). To a certain extent, the material 3K-BC, which has been prepared in a laboratory setting, can serve as a partial replacement for traditional phosphorus fertilisers.

3.2.3 Water retention test

The use of biochar has been demonstrated to enhance soil fertility by increasing soil porosity, water retention and promoting the stability of aggregates (Pandit et al. 2018). As illustrated in Fig. 5D, the water retention capacity of the experimental groups with the addition of biochar did not differ significantly from that of the control group, reaching equilibrium from approximately day 14 onwards. However, during the initial ten-day period, the water retention capacity of the soil was found to be significantly higher in the 3K-BC and BC groups, indicating that the application of biochar can effectively enhance soil water retention even when used for a relatively short duration.

3.3 Potential adsorption mechanisms in soil

The objective of this section is to investigate the potential adsorption mechanism of modified biochar on Pb/Cd under soil conditions. In this experiment, the HHM3 group was subjected to characterisation procedures prior to and following the adsorption of biochar in soil.

The aforementioned characterisation techniques were selected for their suitability for the investigation, and included four common techniques: SEM–EDS, XRD, FT-IR, and XPS. For detailed data analysis, please refer to the supplementary document (in Supporting Information Text S1.7.).

Pb and Cd adsorption by 3K-BC in soil systems occurred primarily through three complementary mechanisms: precipitation, cation exchange, and surface complexation. While our integrated characterization (SEM–EDS/XRD/XPS) and kinetic analyses provide a robust mechanistic framework, we acknowledge that soil-specific interactions—such as microbial mediation and root exudate effects—entail multifaceted processes requiring extended investigation. As shown in Fig. S1-6(A), the advantage of phosphate precipitation was quantified. Cation exchange was verified via K^{+}/Pb^{2+} stoichiometric relationships in Fig. S1-5. Future isotope tracing research is prioritized to address biological/non biological pathways. The current preliminary mechanism research has opened a path for deeper mechanism exploration.

3.4 Percentage of different heavy metal forms in soil

A modified BCR sequential extraction method was employed to examine the morphological characteristics of HMs, specifically investigating alterations in the morphology of Pb and Cd in soil samples with the application of varying rates of biochar. In this method, the HMs were classified into four fractions: acid-soluble, reducible, oxidizable, and residual. The acid-soluble fraction is directly absorbed and utilized by plants and is most easily absorbed and accumulated in organisms. In contrast, the residual fraction is the most stable form and the most difficult to be absorbed and utilized by plants and animals (Li et al. 2022c; Zhang et al. 2023b). As demonstrated in Fig. 6, the morphological distribution of Pb in the control group lacking biochar supplementation was as follows: acid-soluble > residual > oxidizable> reducible. Similarly, the morphological distribution of Cd exhibited the following pattern: acid-soluble > reducible > residual > oxidizable. In comparison to the control group, the addition of 1% and 3% of 3K-BC was observed to effectively reduce the acid-soluble fraction of Pb and Cd. The 3% test group exhibited a more pronounced effect than the 1% test group. The acid-soluble content of both HMs was found to decline significantly in response to an increase in the biochar addition rate. At an application rate of 3%, the acid-soluble fraction of Pb and Cd decreased by 15% and 20%, respectively, for the low concentration HMs group. Conversely, the residual fraction content of the corresponding test group increased by 15% and 14%, respectively. At this juncture, the acid-soluble fraction of Pb and Cd in the high concentration HMs group exhibited a decline of 14% and 27%, respectively. Meanwhile, the residual fraction in the corresponding test group demonstrated an increase of 6% and 25%, respectively. It can be observed that 3K-BC has a superior immobilisation effect on Pb in low-polluted soil, whereas 3K-BC has a more pronounced immobilisation effect on Cd in a high-polluted environment. In conclusion, the application of modified biochar at varying quantities has the potential to transform both Pb and Cd into more stable forms. It was observed that the higher the quantity applied, the more pronounced the effect. This evidence supports the hypothesis that phosphorus-modified biochar has the capacity to immobilise soil HMs.

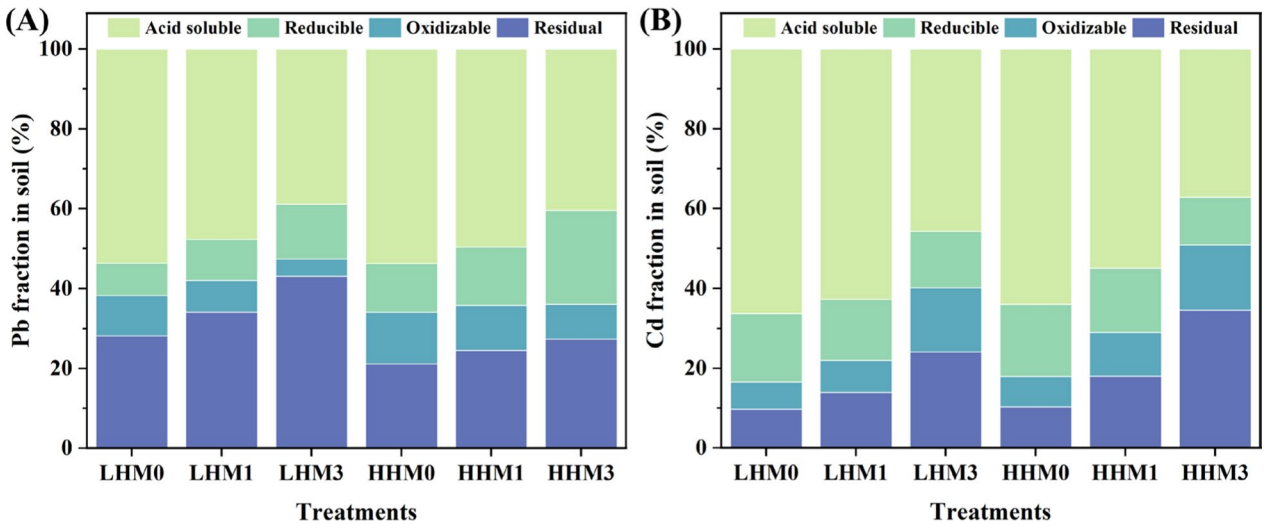


Fig. 6 Speciation distribution of Pb (**A**) and Cd (**B**) in soils amended with 0%, 1% and 3% 3K-BC

3.5 Bioavailability of soil HMs and their potential ecological risk assessment

The bioavailability and leaching toxicity of HMs in contaminated soil were assessed using the $CaCl_2$ and TCLP extraction methods, respectively (Chaudhary and Rao 2024; Serrano et al. 2024). The enhanced mobility and increased bioavailability of HMs in soil can result in greater exposure of plants and other organisms to these contaminants (Wang et al. 2023). The bioavailable HMs content in soil is illustrated in Fig. 7A. In the absence of biochar, the highest levels of HMs extraction were observed in the LHM0 and HHM0 treatment groups, with Pb reaching 3.53 and 20.95 μg kg^{-1} and Cd reaching 11.25 and 62.88 μg kg^{-1}, respectively. This suggested that the soil matrix itself may play a significant role in Pb immobilization (Xia et al. 2021). Furthermore, it was found that with both high and low concentrations of HMs, there was a significant increase in HMs immobilization in the modified soil when 3K-BC was applied. Furthermore, a comparison was made between the measured amounts of different HM contents in the control group without biochar in order to calculate the percentage reduction. It can be observed that when the application rate was 3%, a reduction of 81% for Pb and 91% for Cd was evident at low concentration, and a reduction of 86% for Pb and 93% for Cd was evident at high concentration. It can therefore be concluded that the immobilization efficiency of 3K-BC for Cd was greater than that for Pb.

The TCLP leaching contents are illustrated in Fig. 7B, C. The leached contents of Pb were 112.45 and 219.00 mg kg^{-1} for LHM0 and HHM0, respectively, while the leached contents of Cd were 0.68 and 2.22 mg kg^{-1} for LHM0 and HHM0, respectively. The application of 3K-BC resulted in a significant reduction in the leached contents of HMs, with a notable decrease observed as the application rate increased from 1% to 3%. The Pb content extracted from TCLP was reduced by 24 % and 37% for the 1% and 3% treatments at low concentration, and 21% and 39% at high concentration, respectively, in comparison to the control sample without biochar. Similarly, a reduction of 38% and 44% was observed for Cd at low concentration and 10% and 18% at high concentration, respectively, in the presence of 1% and 3% biochar. A risk assessment of the post-incubation soil was conducted using the *NPI* and the *PI*, and the results are presented in Table S4. With regard to Cd, the *Pi* values decreased from 1.36 to 0.83 and 0.77 with increasing application under low concentration of HMs. This indicated that the soil contamination level changed from light to non-contaminated level. Similarly, following the application of 3K-BC, all *Pi* values in the soil exhibited a marked decline with the increase in applied amount, particularly for Pb at high concentration, from 43.80 (HHM0) to 34.61 (HHM1) and 26.67 (HHM3). This outcome substantiates the efficacy of 3K-BC in mitigating the HM contamination in the soil. Furthermore, the experimental results showed that the pollution level was not reduced for the other groups. This is likely due to the initial concentration of HMs in the experimental setup being so high that it was not possible to ameliorate the soil to a non-polluted level with a limited amount of 3K-BC. The *NPI* value reflects the integrated pollution status of HMs in

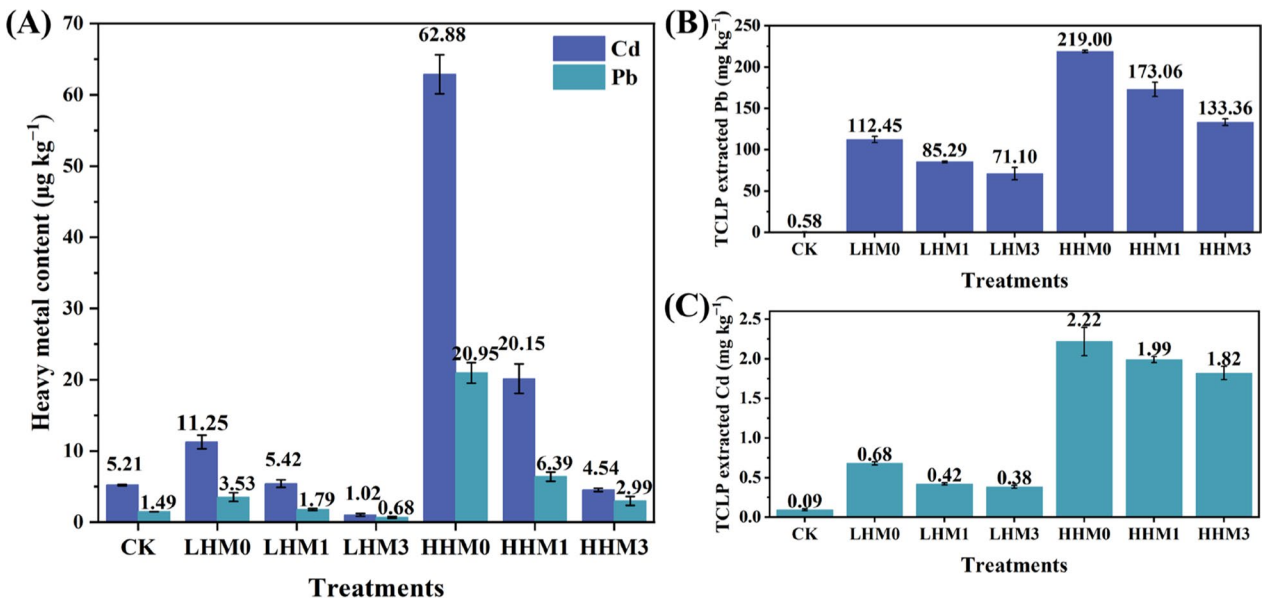


Fig. 7 Analysis of heavy metal immobilization: **A** bioavailability extracted by $CaCl_2$; **B**, **C** leaching toxicity of TCLP extraction

the soil. In the presence of low concentrations of HMs, the *NPI* values demonstrated a notable decline, from 0.96 (LHM0) to 0.35 (LHM1) and 0.31 (LHM3). This observation suggests that the soil exhibited a reduction in contamination, progressing from an elevated alert level to a safer, more stable state. In the remaining experimental groups, the *NPI* values exhibited a decline with the augmentation of application rates under both low and high concentrations of HMs, paralleling the trend observed in the *Pi* values.

The potential ecological risk index may be employed to evaluate the ecological risk level of single or multiple HMs, based on their intrinsic nature and environmental behavioural characteristics (Xia et al. 2020). As illustrated in Table S4, the *Ei* values of HMs in soil, with Pb exhibiting the highest value, indicated that Pb was the most deleterious element in the experimental soil. Following the addition of modified biochar to the soil, a reduction in the *Ei* values of all experimental groups was observed. To illustrate, the *Ei* values of Cd decreased from 40.87 (LHM0) to 24.94 (LHM1) and 23.05 (LHM3) at low concentrations, indicating that the environmental risk was reduced from moderate to low. In all other groups, the *Ei* values exhibited a comparable pattern to that observed in the Nemerow index. In other words, the addition of 3K-BC at either high or low concentrations has the potential to reduce the ecological risk associated with HMs in soil. It is noteworthy that in the high concentration pollution test group, despite the reduction in ecological risk of Pb and Cd resulting from the addition of 3% of the material, the index remains high. Furthermore, in the low concentration group, the integrated assessment index *PI* values were 153.32, 110.23, and 94.16, thus classified as low risk. Following the addition of 3K-BC to the high concentration group, the soil was observed to transition from a high-risk to a medium-risk classification. In conclusion, 3K-BC is an immobilization material that has been demonstrated to effectively reduce the ecological risk of Pb and Cd. Additionally, the use of excessively high or low concentrations of heavy metals will reduce the discriminative power of subsequent pot experiment results. Therefore, the results of the ecological risk assessment experiment can also be used to help inform the setting of HM concentrations in pot experiments.

3.6 Effect of biochar on the growth of *Ligusticum chuanxiong*

3.6.1 Plant yield

The impact of modified biochar on the yield during the growth of *Ligusticum chuanxiong* is illustrated in Fig. 8A. In the case of the blank soil group BK and 1% BC-BK, the addition of 1% 3K-BC resulted in a 10% increase in the weight of roots and a 3% increase in the weight of leaves of *Ligusticum chuanxiong*, while the weight of stems remained largely unchanged. A comparison of the BK and 0% BC-HM groups revealed that the addition of HMs had an inhibitory effect on the growth of various parts of the plant *Ligusticum chuanxiong*. The absorption of nutrients and photosynthesis in roots in soil–plant systems can be disrupted by Pb and Cd, which consequently impede the growth of plants (Chen et al. 2024a; Ur Rahman et al. 2024). In comparison to BK, the roots and leaves of 1% BC-HM exhibited an increase of approximately 28% and 18%, respectively, while the weight of the stems decreased by approximately 17%. Under the condition

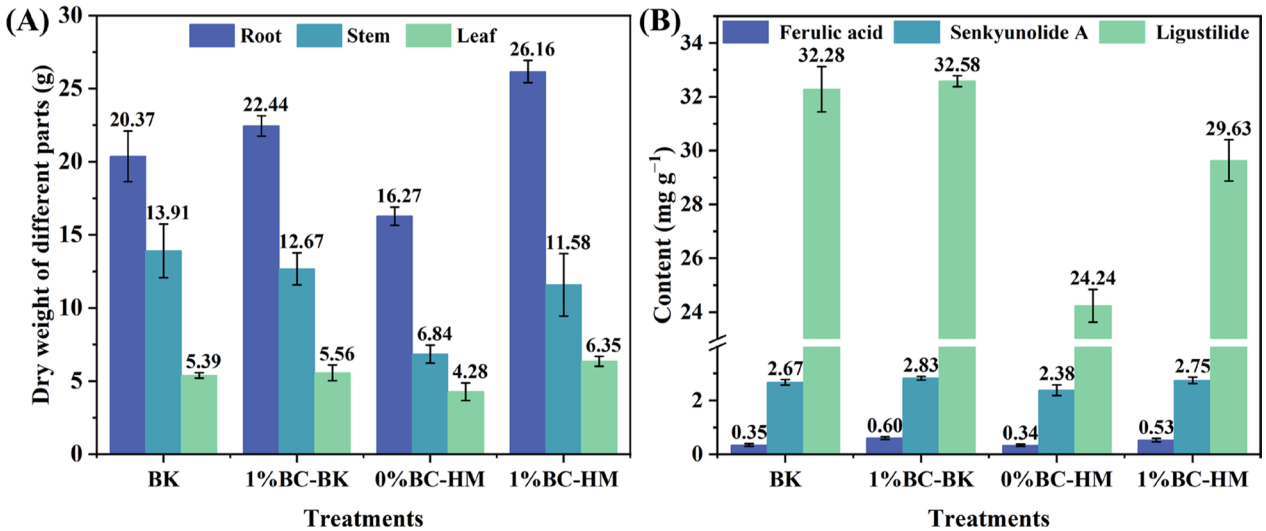


Fig. 8 **A** Dry weight of different plant parts; **B** contents of ferulic acid, senkyunolide A and ligustilide in different groups of plants

of HM pollution, the yield of *Ligusticum chuanxiong* in the experimental group increased by 61.0%. It has been demonstrated that the utilization of biochar can facilitate enhanced plant growth (Ghandali et al. 2024; Huang et al. 2024). The experimental results demonstrated that 3K-BC facilitated the growth of *Ligusticum chuanxiong*, particularly the roots of the medicinal parts. It is hypothesised that the biochar material is rich in phosphorus and potassium, essential nutrients for plant growth, which can enhance the efficacy of chemical fertilizers. The utilization of biochar as an organic substitute for synthetic waste for the enhancement of soil quality is also a significant area of interest for agricultural scientists in recent years (Bilias et al. 2023; Hou et al. 2022).

3.6.2 Medicinal ingredients

The contents of ferulic acid, senkyunolide A and ligustilide were determined in the roots of different groups of traditional medicinal parts, as illustrated in Fig. 8B. In the context of blank soil, the application of 1% 3K-BC was observed to exert a discernible influence on the accumulation of ferulic acid and senkyunolide A, while the content of ligustilide remained largely unaltered. The addition of HMs to the soil resulted in the inhibition of the three effective components. The concentrations of ferulic acid, senkyunolide A and ligustilide were found to be 0.34, 2.38 and 24.24 mg g^{-1}, respectively. It is notable that the inhibitory effect of HMs on ligustilide is particularly pronounced. The findings indicated that HMs Pb and Cd exerted an inhibitory impact on the synthesis of active compounds in *Ligusticum chuanxiong*. This phenomenon may be attributed to the accumulation of HMs within *Ligusticum chuanxiong*, which in turn impedes its normal physiological and biochemical processes (Zeng et al. 2020; Zhang et al. 2023c). The addition of 1% 3K-BC to soil contaminated with HMs resulted in a certain degree of mitigation of the inhibitory effect on the three active ingredients, as evidenced by an increase in their content. To illustrate, the concentration of ligustilide increased from 24.24 to 29.63 mg g^{-1}. Under the condition of HM pollution, the total effective components of *Ligusticum chuanxiong* in the experimental group increased by 22.1%. The experiment demonstrated that 3K-BC had a beneficial impact on the pharmacodynamic components of *Ligusticum chuanxiong*, and could mitigate the adverse effects of HMs in the soil to a certain extent.

3.6.3 Distribution of HMs in organisms

The distribution of HMs in the different parts of *Ligusticum chuanxiong* is illustrated in Table S5. The results showed that the sensitivity of *Ligusticum chuanxiong* to Cd was higher in the 0%BC-HM and 1%BC-HM groups. The highest total concentrations of Pb and Cd in the plants were 17.41 and 14.85 mg kg^{-1}, respectively. At the same time, Pb was mainly distributed in the roots of the plants, while Cd was mainly distributed in the stems of the plants. The same distribution pattern was observed in each experimental group. With the addition of 3K-BC, the concentration of Cd in each part of *Ligusticum chuanxiong* was significantly reduced, while only the stem part concentration of Pb was significantly reduced ($p < 0.05$). Of the four groups, the group with 0% BC-HM exhibited the highest accumulation of HMs. In accordance with the existing literature, the *BCF* values of Cd in each group were all greater than 1, indicating that Cd was relatively enriched in *Ligusticum chuanxiong* (Zeng et al. 2020). *Ligusticum chuanxiong* showed an enrichment effect on HMs, especially Cd. The *BCF* values for Pb were less than 1, indicating that *Ligusticum chuanxiong* had not yet reached the level of enrichment.

The *TF* values of Pb and Cd exhibited no statistically significant difference in the context of HM pollution between 0% BC-HM and 1% BC-HM. It is speculated that the addition of biochar will inhibit the transport capacity and enrichment ability of *Ligusticum chuanxiong* roots for HMs. In conclusion, the application of 3K-BC resulted in a slight reduction in the Pb and Cd content in the *Ligusticum chuanxiong* root, stem, and leaf. The data presented here may be used as a reference for the development of a planting technique for *Ligusticum chuanxiong* that facilitates the removal of HMs.

4 Conclusion

This study explored the use of 3K-BC biochar, derived from Traditional Chinese medicinal herb residues (*Salvia miltiorrhiza* residue), to remediate Pb/Cd contamination in water and soil. Adsorption experiments revealed a chemical, monolayer process (pseudo-second-order/Langmuir models) with high capacities (361.82 mg g^{-1} Pb; 123.03 mg g^{-1} Cd), driven by physical adsorption, precipitation, complexation, and cation exchange. In soil, 1% 3K-BC enhanced urease and phosphatase activity, but 3% inhibited phosphatase. BCR analysis confirmed 3K-BC converted acid-soluble Pb/Cd into stable forms, reducing bioavailability and ecological risks. Pot trials showed 3K-BC improved *Ligusticum chuanxiong* growth, medicinal quality, and reduced HM uptake. Although conducting a systematic evaluation of cost-effectiveness and long-term stability remains challenging, this study demonstrates significant advantages: (1) Circular resource utilization of waste TCM residues eliminates feedstock costs; (2) Dual functionality achieves simultaneous heavy metal immobilization (>93% Cd bioavailability reduction) and plant growth promotion (61% *chuanxiong* yield increase); (3) After 50 days of

incubation, the residual conversion rates of heavy metals in soil were up to 25% (Cd) and 15% (Pb). Current limitations involve plant-specific validation (Apiaceae family) and scalability, which will guide future studies on broader crop applicability and field-scale economics. The data that support the findings of this study are available from the corresponding author upon reasonable request.

Supplementary Information

The online version contains supplementary material available at https://doi.org/10.1007/s42773-025-00540-5.

Additional file 1.

Author contributions

Jiandan Yuan: Methodology, Data curation, Formal analysis, Writing—original draft, visualization. Yanling Liu, Qian He, Zhenghua Li, and Hongting Wen: Methodology, Formal analysis, Writing—review. Ruifeng Lin and Tianzhe Chu: Investigation, Writing—review & editing. Cheng Peng and Chuan Zheng: Resources, Funding acquisition, Supervision. Hulan Chen and Yuzhu Tan: Conceptualization, Project administration, Supervision, Writing—review and editing. All the authors read and approved the final manuscript.

Funding

Sichuan Science and Technology Program, 2023NSFSC1994, 2025NSFSC2160, National Interdisciplinary Innovation Team of Traditional Chinese Medicine, ZYYCXTD-D-202209, National Key R&D Program of China, 2025YFC3509100.

Declaration of generative AI and AI-assisted technologies in the writing process

During the preparation of this work, the author(s) used AI embellishment in order to improve the readability and language of manuscripts in the writing process.

Declarations

Competing interests

The authors declare that they have no known competing financial interests or personal relationships that could have appeared to influence the work reported in this paper.

Author details

[1]School of Pharmacy, Chinese Medicine Germplasm Resources Innovation and Effective Uses Key Laboratory of Sichuan Province, Key Laboratory of Standardization of Chinese Medicine (Chengdu University of Traditional Chinese Medicine), Ministry of Education, Chengdu University of Traditional Chinese Medicine, Chengdu 611137, China. [2]Chongqing University of Chinese Medicine, Chongqing 402760, China. [3]TCM Regulating Metabolic Diseases Key Laboratory of Sichuan Province, Hospital of Chengdu University of Traditional Chinese Medicine, Chengdu 610072, China. [4]Sichuan Provincial Engineering Research Center of Innovative Re-development of Famous Classical Formulas, Tianfu TCM Innovation Harbour, Chengdu University of Traditional Chinese Medicine, Chengdu 611930, China. [5]College of Medical Technology, Chengdu University of Traditional Chinese Medicine, Chengdu 611137, China.

Received: 13 April 2025 Revised: 19 October 2025 Accepted: 28 October 2025
Published: 16 February 2026

References

Abdullayev E, Vakili AH, Amr SSA, Alazaiza MYD (2024) Navigating heavy metal removal: Insights into advanced treatment technologies for wastewater: a review. Global Nest J 26(6):1–12. https://doi.org/10.30955/gnj.006247

Ahmad Z, Gao B, Mosa A, Yu HW, Yin XQ, Bashir A, Ghoveisi H, Wang SS (2018) Removal of Cu(II), Cd(II) and Pb(II) ions from aqueous solutions by biochars derived from potassium-rich biomass. J Clean Prod 180:437–449. https://doi.org/10.1016/j.jclepro.2018.01.133

Ayach J, El Malti W, Duma L, Lalevée J, Al Ajami M, Hamad H, Hijazi A (2024) Comparing conventional and advanced approaches for heavy metal removal in wastewater treatment: an in-depth review emphasizing filter-based strategies. Polymers. https://doi.org/10.3390/polym16141959

Aziz KHH (2024) Removal of toxic heavy metals from aquatic systems using low-cost and sustainable biochar: a review. Desalin Water Treat. https://doi.org/10.1016/j.dwt.2024.100757

Behbahani ES, Dashtian K, Ghaedi M (2021) Fe(3)O(4)-FeMoS(4): promise magnetite LDH-based adsorbent for simultaneous removal of Pb (II), Cd (II), and Cu (II) heavy metal ions. J Hazard Mater 410:124560. https://doi.org/10.1016/j.jhazmat.2020.124560

Berslin D, Reshmi A, Sivaprakash B, Rajamohan N, Kumar PS (2022) Remediation of emerging metal pollutants using environment friendly biochar-review on applications and mechanism. Chemosphere. https://doi.org/10.1016/j.chemosphere.2021.133384

Bilias F, Kalderis D, Richardson C, Barbayiannis N, Gasparatos D (2023) Biochar application as a soil potassium management strategy: A review. Sci Total Environ 858(Pt 1):159782. https://doi.org/10.1016/j.scitotenv.2022.159782

Bukhari A, Ijaz I, Nazir A, Hussain S, Zain H, Gilani E, Lfseisi AA, Ahmad H (2024) Functionalization of *Shorea faguetiana* biochar using Fe(2)O(3) nanoparticles and MXene for rapid removal of methyl blue and lead from both single and binary systems. RSC Adv 14(6):3732–3747. https://doi.org/10.1039/d3ra07250a

Chaudhary H, Rao KS (2024) Impact of biochar produced at different pyrolysis conditions on heavy metal contaminated soil. Environ Geochem Health. https://doi.org/10.1007/s10653-024-02092-2

Chen H, Li W, Wang J, Xu H, Liu Y, Zhang Z, Li Y, Zhang Y (2019) Adsorption of cadmium and lead ions by phosphoric acid-modified biochar generated from chicken feather: selective adsorption and influence of dissolved organic matter. Bioresour Technol. https://doi.org/10.1016/j.biortech.2019.121948

Chen X, Zhu X, Fan G, Wang X, Li H, Li H, Xu X (2022) Enhanced adsorption of Pb(II) by phosphorus-modified chicken manure and Chinese medicine residue co-pyrolysis biochar. Microsc Res Tech 85(11):3589–3599. https://doi.org/10.1002/jemt.24210

Chen X, Ran Z, Li R, Duan W, Song Z, Fang L, Guo L, Zhou J (2024a) Biochar reduces the cadmium content of *Panax quinquefolium* L. by improving rhizosphere microecology. Sci Total Environ. https://doi.org/10.1016/j.scitotenv.2024.170005

Chen Y, Yang W, Zou Y, Wu Y, Mao W, Zhang J, Zia-Ur-Rehman M, Wang B, Wu P (2024b) Quantification of the effect of biochar application on heavy metals in paddy systems: impact, mechanisms and future prospects. Sci Total Environ 912:168874. https://doi.org/10.1016/j.scitotenv.2023.168874

Cui H, Dong T, Hu L, Xia R, Zhou J, Zhou J (2022) Adsorption and immobilization of soil lead by two phosphate-based biochars and phosphorus release risk assessment. Sci Total Environ 824:153957. https://doi.org/10.1016/j.scitotenv.2022.153957

Das NK, Navarathna CM, Alchouron J, Arwenyo B, Rahman S, Hoffman B, Lee K, Stokes S, Anderson R, Perez F, Mohan D, Pittman CU Jr, Mlsna T (2023) Efficient aqueous molybdenum removal using commercial Douglas fir biochar and its iron oxide hybrids. J Hazard Mater 443(Pt B):130257. https://doi.org/10.1016/j.jhazmat.2022.130257

Gao R, Fu Q, Hu H, Wang Q, Liu Y, Zhu J (2019) Highly-effective removal of Pb by co-pyrolysis biochar derived from rape straw and orthophosphate. J Hazard Mater 371:191–197. https://doi.org/10.1016/j.jhazmat.2019.02.079

Gao R, Hu H, Fu Q, Li Z, Xing Z, Ali U, Zhu J, Liu Y (2020) Remediation of Pb, Cd, and Cu contaminated soil by co-pyrolysis biochar derived from rape straw and orthophosphate: speciation transformation, risk evaluation and mechanism inquiry. Sci Total Environ. https://doi.org/10.1016/j.scitotenv.2020.139119

Ghandali MV, Safarzadeh S, Ghasemi-Fasaei R, Zeinali S (2024) Heavy metals immobilization and bioavailability in multi-metal contaminated soil under ryegrass cultivation as affected by ZnO and MnO2 nanoparticle-modified biochar. Sci Rep. https://doi.org/10.1038/s41598-024-61270-5

Gu P, Zhang Y, Xie H, Wei J, Zhang X, Huang X, Wang J, Lou X (2020) Effect of cornstalk biochar on phytoremediation of Cd-contaminated soil by *Beta*

vulgaris var. *cicla* L. Ecotoxicol Environ Saf 205:111144. https://doi.org/10.1016/j.ecoenv.2020.111144
Hakanson L (1980) An ecological risk index for aquatic pollution control. A sedimentological approach. Water Res 14(8):975–1001. https://doi.org/10.1016/0043-1354(80)90143-8
Han Q, Liu F, Wang C, Tang Z, Peng C, Tan Y (2023) Polyethylene glycol functionalized Fe3O4@MIL-101(Cr) for the efficient removal of heavy metals from *Ligusticum chuanxiong* Hort. Arab J Chem 16(4):104635. https://doi.org/10.1016/j.arabjc.2023.104635
Harvey OR, Herbert BE, Rhue RD, Kuo L-J (2011) Metal interactions at the biochar-water interface: energetics and structure-sorption relationships elucidated by flow adsorption microcalorimetry. Environ Sci Technol 45(13):5550–5556. https://doi.org/10.1021/es104401h
Herath A, Layne CA, Perez F, Hassan EIB, Pittman CU, Mlsna TE (2021) KOH-activated high surface area Douglas Fir biochar for adsorbing aqueous Cr(VI), Pb(II) and Cd(II). Chemosphere 269:128409. https://doi.org/10.1016/j.chemosphere.2020.128409
Hou J, Pugazhendhi A, Sindhu R, Vinayak V, Thanh NC, Brindhadevi K, Lan Chi NT, Yuan D (2022) An assessment of biochar as a potential amendment to enhance plant nutrient uptake. Environ Res. https://doi.org/10.1016/j.envres.2022.113909
Hu XL, Long L, Gong TJ, Zhang JQ, Yan JP, Xue YW (2020) Enhanced alginate-based microsphere with the pore-forming agent for efficient removal of Cu(II). Chemosphere. https://doi.org/10.1016/j.chemosphere.2019.124860
Huang K, Hu C, Tan Q, Yu M, Shabala S, Yang L, Sun X (2022) Highly efficient removal of cadmium from aqueous solution by ammonium polyphosphate-modified biochar. Chemosphere. https://doi.org/10.1016/j.chemosphere.2022.135471
Huang Y, Liu T, Liu J, Xiao X, Wan Y, An H, Luo X, Luo S (2024) Exceptional anti-toxic growth of water spinach in arsenic and cadmium co-contaminated soil remediated using biochar loaded with *Bacillus aryabhattai*. J Hazard Mater. https://doi.org/10.1016/j.jhazmat.2024.133966
Jin Q, Wang Z, Feng Y, Kim YT, Stewart AC, O'Keefe SF, Neilson AP, He Z, Huang H (2020) Grape pomace and its secondary waste management: biochar production for a broad range of lead (Pb) removal from water. Environ Res 186:109442. https://doi.org/10.1016/j.envres.2020.109442
Khalid S, Shahid M, Niazi NK, Murtaza B, Bibi I, Dumat C (2017) A comparison of technologies for remediation of heavy metal contaminated soils. J Geochem Explor 182:247–268. https://doi.org/10.1016/j.gexplo.2016.11.021
Kong QH, Niu YS, Feng H, Yu XF, Wang BK, Liu X, Chen YR, Wang FL, Tian JZ, Zhou HL (2024) *Ligusticum chuanxiong* Hort.: a review of its phytochemistry, pharmacology, and toxicology. J Pharm Pharmacol. https://doi.org/10.1093/jpp/rgae105
Landrigan PJ, Fuller R, Acosta NJR, Adeyi O, Arnold R, Basu N, Baldé AB, Bertollini R, Bose-O'Reilly S, Boufford JI, Breysse PN, Chiles T, Mahidol C, Coll-Seck AM, Cropper ML, Fobil J, Fuster V, Greenstone M, Haines A, Hanrahan D, Hunter D, Khare M, Krupnick A, Lanphear B, Lohani B, Martin K, Mathiasen KV, McTeer MA, Murray CJL, Ndahimananjara JD, Perera F, Potocnik J, Preker AS, Ramesh J, Rockström J, Salinas C, Samson LD, Sandilya K, Sly PD, Smith KR, Steiner A, Stewart RB, Suk WA, van Schayck OCP, Yadama GN, Yumkella K, Zhong M (2018) The Lancet Commission on pollution and health. Lancet 391(10119):462–512. https://doi.org/10.1016/S0140-6736(17)32345-0
Li B, Yang L, Wang CQ, Zhang QP, Liu QC, Li YD, Xiao R (2017) Adsorption of Cd(II) from aqueous solutions by rape straw biochar derived from different modification processes. Chemosphere 175:332–340. https://doi.org/10.1016/j.chemosphere.2017.02.061
Li H, Li Y, Xu Y, Lu X (2020) Biochar phosphorus fertilizer effects on soil phosphorus availability. Chemosphere 244:125471. https://doi.org/10.1016/j.chemosphere.2019.125471
Li H, Jiang Q, Li R, Zhang B, Zhang J, Zhang Y (2022a) Passivation of lead and cerium in soil facilitated by biochar-supported phosphate-doped ferrihydrite: mechanisms and microbial community evolution. J Hazard Mater. https://doi.org/10.1016/j.jhazmat.2022.129090
Li H, Jiang Q, Zhang J, Wang Y, Zhang Y (2022b) Synchronization adsorption of Pb(II) and Ce(III) by biochar supported phosphate-doped ferrihydrite in aqueous solution: adsorption efficiency and mechanisms. Colloids Surf A Physicochem Eng Asp. https://doi.org/10.1016/j.colsurfa.2022.129230
Li J, Xia C, Cheng R, Lan J, Chen F, Li X, Li S, Chen J, Zeng T, Hou H (2022c) Passivation of multiple heavy metals in lead–zinc tailings facilitated by straw biochar-loaded N-doped carbon aerogel nanoparticles: mechanisms and microbial community evolution. Sci Total Environ 803:149866. https://doi.org/10.1016/j.scitotenv.2021.149866
Li S, Luo C, Yan F, Yang Y, Guo B, Wang L, Xu S, Wu F, Ji P (2023) Remediation of Pb(II) and Cd(II) in polluted waters with calcium thioglycolate-modified straw biochar. Environ Pollut 338:122638. https://doi.org/10.1016/j.envpol.2023.122638
Li SQ, Yan X, Zhang MJ, Sun Q, Zhu XZ (2024) Microbial remediation technology for heavy metal contamination of mine soil. Chemoecology 34(2):47–59. https://doi.org/10.1007/s00049-024-00399-1
Liao Z, Wu S, Xie H, Chen F, Yang Y, Zhu R (2023) Effect of phosphate on cadmium immobilized by microbial-induced carbonate precipitation: Mobilization or immobilization? J Hazard Mater 443(Pt B):130242–130249. https://doi.org/10.1016/j.jhazmat.2022.130242
Lin W, Zhou J, Sun S (2023) Cadmium and lead removal by Mg/Fe bimetallic oxide-loaded sludge-derived biochar: batch adsorption, kinetics, and mechanism. Environ Sci Pollut Res Int. https://doi.org/10.1007/s11356-023-28574-x
Liu L, Huang Y, Meng Y, Cao J, Hu H, Su Y, Dong L, Tao S, Ruan R (2020) Investigating the adsorption behavior and quantitative contribution of Pb2+ adsorption mechanisms on biochars by different feedstocks from a fluidized bed pyrolysis system. Environ Res 187:109609. https://doi.org/10.1016/j.envres.2020.109609
Liu L, Fan S, Wang Z, Hu J (2024) Chemical speciation distribution, desorption characteristics, and quantitative adsorption mechanisms of cadmium/lead ions adsorbed on biochars. Arab J Chem. https://doi.org/10.1016/j.arabjc.2024.105669
Lu J, Li Y, Cai Y, Jiang P, Yu B (2023) Co-incorporation of hydrotalcite and starch into biochar-based fertilizers for the synthesis of slow-release fertilizers with improved water retention. Biochar. https://doi.org/10.1007/s42773-023-00242-w
Luo J, Sun M, Ritt CL, Liu X, Pei Y, Crittenden JC, Elimelech M (2019) Tuning Pb(II) adsorption from aqueous solutions on ultrathin iron oxychloride (FeOCl) nanosheets. Environ Sci Technol 53(4):2075–2085. https://doi.org/10.1021/acs.est.8b07027
Nguyen T-B, Sherpa K, Bui X-T, Nguyen V-T, Vo T-D-H, Ho H-T-T, Chen C-W, Dong C-D (2023) Biochar for soil remediation: a comprehensive review of current research on pollutant removal. Environ Pollut. https://doi.org/10.1016/j.envpol.2023.122571
Nigam N, Khare P, Ahsan M, Yadav V, Shanker K, Singh RP, Panday V, Das P, Singh A, Yadav R, Tripathi P, Sinam G, Shukla AK, Karak T (2021) Biochar amendment reduced the risk associated with metal uptake and improved metabolite content in medicinal herbs. Physiol Plant. https://doi.org/10.1111/ppl.13393
Pandit NR, Mulder J, Hale SE, Martinsen V, Schmidt HP, Cornelissen G (2018) Biochar improves maize growth by alleviation of nutrient stress in a moderately acidic low-input Nepalese soil. Sci Total Environ 625:1380–1389. https://doi.org/10.1016/j.scitotenv.2018.01.022
Qu ZM, Chen Q, Yin SH, Feng HJ, Liu YL, Li CL (2024) Effects of drip irrigation coupled with controlled release potassium fertilizer on maize growth and soil properties. Agric Water Manage. https://doi.org/10.1016/j.agwat.2024.108948
Serrano MF, Lopez JE, Henao N, Saldarriaga JF (2024) Phosphorus-loaded biochar-assisted phytoremediation to immobilize cadmium, chromium, and lead in soils. ACS Omega 9(3):3574–3587. https://doi.org/10.1021/acsomega.3c07433
Song P, Ma W, Gao X, Ai S, Wang J, Liu W (2022) Remediation mechanism of Cu, Zn, As, Cd, and Pb contaminated soil by biochar-supported nanoscale zero-valent iron and its impact on soil enzyme activity. J Clean Prod. https://doi.org/10.1016/j.jclepro.2022.134510
Subramanian P, Pandian K, Pakkiyam S, Dhanuskodi KV, Annamalai S, Chidambaram PP, Mustaffa MRA (2024) Biochar for heavy metal cleanup in soil and water: a review. Biomass Convers Biorefinery. https://doi.org/10.1007/s13399-024-05989-1
Sun E, Zhang Y, Xiao Q, Li H, Qu P, Yong C, Wang B, Feng Y, Huang H, Yang L, Hunter C (2022) Formable porous biochar loaded with La-Fe(hydr) oxides/montmorillonite for efficient removal of phosphorus in wastewater: process and mechanisms. Biochar. https://doi.org/10.1007/s42773-022-00177-8
Ullah MH, Rahman MJ (2024) Adsorptive removal of toxic heavy metals from wastewater using water hyacinth and its biochar: a review. HELIYON 10(17):e36869. https://doi.org/10.1016/j.heliyon.2024.e36869

Ur Rahman S, Qin A, Zain M, Mushtaq Z, Mehmood F, Riaz L, Naveed S, Ansari MJ, Saeed M, Ahmad I, Shehzad M (2024) Pb uptake, accumulation, and translocation in plants: plant physiological, biochemical, and molecular response: a review. Heliyon. https://doi.org/10.1016/j.heliyon.2024.e27724

Wang Q, Yang Z (2016) Industrial water pollution, water environment treatment, and health risks in China. Environ Pollut 218:358–365. https://doi.org/10.1016/j.envpol.2016.07.011

Wang T, Li C, Wang C, Wang H (2018) Biochar/MnAl-LDH composites for Cu (**II**) removal from aqueous solution. Colloids Surf A Physicochem Eng Asp 538:443–450

Wang X, Dong G, Liu X, Zhang S, Li C, Lu X, Xia T (2020) Poly-γ-glutamic acid-producing bacteria reduced Cd uptake and effected the rhizosphere microbial communities of lettuce. J Hazard Mater 398:123146. https://doi.org/10.1016/j.jhazmat.2020.123146

Wang Y, Wang L, Li Z, Yang D, Xu J, Liu X (2021) Mgo-laden biochar enhances the immobilization of Cd/Pb in aqueous solution and contaminated soil. Biochar 3(2):175–188. https://doi.org/10.1007/s42773-020-00080-0

Wang Q, Duan CJ, Xu CY, Geng ZC (2022) Efficient removal of Cd(II) by phosphate-modified biochars derived from apple tree branches: processes, mechanisms, and application. Sci Total Environ 819:152876. https://doi.org/10.1016/j.scitotenv.2021.152876

Wang Z, Zhang Y, Sun S, Hu J, Zhang W, Liu H, He H, Huang J, Wu F, Zhou Y, Huang F, Chen L (2023) Effects of four amendments on cadmium and arsenic immobilization and their exposure risks from pakchoi consumption. Chemosphere. https://doi.org/10.1016/j.chemosphere.2023.139844

Wang A, Wu M, Li Z, Zhou Y, Zhu F, Huang Z (2024a) Utilizing different types of biomass materials to modify steel slag for the preparation of composite materials used in the adsorption and solidification of Pb in solutions and soil. Sci Total Environ 914:170023. https://doi.org/10.1016/j.scitotenv.2024.170023

Wang C, Qiao J, Yuan J, Tang Z, Chu T, Lin R, Wen H, Zheng C, Chen H, Xie H, Peng C, Tan Y (2024b) Novel chitosan-modified biochar prepared from a Chinese herb residue for multiple heavy metals removal: characterization, performance and mechanism. Bioresour Technol 402:130830. https://doi.org/10.1016/j.biortech.2024.130830

Wu J, Wang T, Wang J, Zhang Y, Pan WP (2021) A novel modified method for the efficient removal of Pb and Cd from wastewater by biochar: enhanced the ion exchange and precipitation capacity. Sci Total Environ 754:142150. https://doi.org/10.1016/j.scitotenv.2020.142150

Xia Y, Luo H, Li D, Chen Z, Yang S, Liu Z, Yang T, Gai C (2020) Efficient immobilization of toxic heavy metals in multi-contaminated agricultural soils by amino-functionalized hydrochar: performance, plant responses and immobilization mechanisms. Environ Pollut. https://doi.org/10.1016/j.envpol.2020.114217

Xia Y, Li Y, Sun Y, Miao W, Liu Z (2021) Co-pyrolysis of corn stover with industrial coal ash for in situ efficient remediation of heavy metals in multi-polluted soil. Environ Pollut 289:117840. https://doi.org/10.1016/j.envpol.2021.117840

Xie Y, Liu H, Xie X, Li Y, Peng F, Zhao Y, Xu H (2023) Active ingredients biosynthesis and genic response of traditional Chinese medicine *Ligusticum sinense* cv. Chuanxiong under different cadmium level. Ind Crops Prod. https://doi.org/10.1016/j.indcrop.2023.117074

Yang S, Wen Q, Chen Z (2021) Effect of KH(2)PO(4)-modified biochar on immobilization of Cr, Cu, Pb, Zn and as during anaerobic digestion of swine manure. Bioresour Technol 339:125570. https://doi.org/10.1016/j.biortech.2021.125570

Yang F, Lv J, Zhou Y, Wu S, Sima J (2023) Co-pyrolysis of biomass and phosphate tailing to produce potential phosphorus-rich biochar: efficient removal of heavy metals and the underlying mechanisms. Environ Sci Pollut Res Int 30(7):17804–17816. https://doi.org/10.1007/s11356-022-23128-z

Yilmaz C, Guzel F (2021) Sorptive removal of copper(II) from water by biochar produced from a novel sustainable feedstock: wild herbs. Environ Sci Pollut Res 28(1):995–1005. https://doi.org/10.1007/s11356-020-10560-2

Yin D, Wang X, Chen C, Peng B, Tan C, Li H (2016) Varying effect of biochar on Cd, Pb and As mobility in a multi-metal contaminated paddy soil. Chemosphere 152:196–206. https://doi.org/10.1016/j.chemosphere.2016.01.044

Yuan J, Wang C, Tang Z, Chu T, Zheng C, Han Q, Chen H, Tan Y (2024) Biochar derived from traditional Chinese medicine residues: an efficient adsorbent for heavy metal Pb(II). Arab J Chem. https://doi.org/10.1016/j.arabjc.2024.105606

Zeng J, Li X, Wang X, Zhang K, Wang Y, Kang H, Chen G, Lan T, Zhang Z, Yuan S, Wang C, Zhou Y (2020) Cadmium and lead mixtures are less toxic to the Chinese medicinal plant *Ligusticum chuanxiong* Hort. than either metal alone. Ecotoxicol Environ Saf. https://doi.org/10.1016/j.ecoenv.2020.110342

Zhang G, Liu X, Gao M, Song Z (2020a) Effect of Fe–Mn–Ce modified biochar composite on microbial diversity and properties of arsenic-contaminated paddy soils. Chemosphere. https://doi.org/10.1016/j.chemosphere.2020.126249

Zhang H, Shao J, Zhang S, Zhang X, Chen H (2020b) Effect of phosphorus-modified biochars on immobilization of Cu (II), Cd (II), and As (V) in paddy soil. J Hazard Mater 390:121349. https://doi.org/10.1016/j.jhazmat.2019.121349

Zhang A, Liu J, Yang Y, Yu Y, Wu D (2023a) Experimental and theoretical studies on the adsorption performance of lead by thermal pre-activation and phosphate modified kaolin sorbent. Chem Eng J. https://doi.org/10.1016/j.cej.2022.138762

Zhang L, Hu J, Li C, Chen Y, Zheng L, Ding D, Shan S (2023b) Synergistic mechanism of iron manganese supported biochar for arsenic remediation and enzyme activity in contaminated soil. J Environ Manage 347:119127. https://doi.org/10.1016/j.jenvman.2023.119127

Zhang Z, Zhong L, Xiao W, Du Y, Han G, Yan Z, He D, Zheng C (2023c) Transcriptomics combined with physiological analysis reveals the mechanism of cadmium uptake and tolerance in *Ligusticum chuanxiong* Hort. under cadmium treatment. Front Plant Sci. https://doi.org/10.3389/fpls.2023.1263981

Zhao F-J, Ma Y, Zhu Y-G, Tang Z, McGrath SP (2014) Soil contamination in China: current status and mitigation strategies. Environ Sci Technol 49(2):750–759. https://doi.org/10.1021/es5047099

Zhao L, Guan H, Wang R, Wang H, Li Z, Li W, Xiang P, Xu W (2021) Effects of tobacco stem-derived biochar on soil properties and bacterial community structure under continuous cropping of *Bletilla striata*. J Soil Sci Plant Nutr 21(2):1318–1328. https://doi.org/10.1007/s42729-021-00442-y

Zhao H, Wu Y, Lan X, Yang Y, Wu X, Du L (2022) Comprehensive assessment of harmful heavy metals in contaminated soil in order to score pollution level. Sci Rep. https://doi.org/10.1038/s41598-022-07602-9

Zhou QQ, Yang N, Li YZ, Ren B, Ding XH, Bian HL, Yao X (2020) Total concentrations and sources of heavy metal pollution in global river and lake water bodies from 1972 to 2017. Glob Ecol Conserv. https://doi.org/10.1016/j.gecco.2020.e00925

Zhou C, Song X, Wang Y, Wang H, Ge S (2022) The sorption and short-term immobilization of lead and cadmium by nano-hydroxyapatite/biochar in aqueous solution and soil. Chemosphere 286:131810. https://doi.org/10.1016/j.chemosphere.2021.131810

Zhou Y, Lan Y, Short MD, Shi J, Zhang Q, Xu J, Qian G (2023) Effective use of sugarcane-bagasse-derived KOH-activated biochar for remediating norfloxacin-contaminated water. Toxics. https://doi.org/10.3390/toxics11110908

Zong Y, Xiao Q, Lu S (2021) Biochar derived from cadmium-contaminated rice straw at various pyrolysis temperatures: cadmium immobilization mechanisms and environmental implication. Bioresour Technol 321:124459. https://doi.org/10.1016/j.biortech.2020.124459